Impact of imposed mode 2 laser drive asymmetry on inertial confinement fusion implosions

M. Gatu Johnson[1], B.D. Appelbe,[2] J.P. Chittenden,[2] A. Crilly,[2] J. Delettrez,[3] C. Forrest,[3] J.A. Frenje,[1] V.Yu. Glebov,[3] W. Grimble,[3] B.M. Haines,[4] I. Igumenshchev,[3] R. Janezic,[3] J.P. Knauer,[3] B. Lahmann,[1] F.J. Marshall,[3] T. Michel,[3] F.H. Séguin,[1] C. Stoeckl,[3] C. Walsh,[2] A.B. Zylstra,[4] R.D. Petrasso[1]

[1]*Massachusetts Institute of Technology, Cambridge, MA 02139, USA*
[2]*Centre for Inertial Fusion Studies, The Blackett Laboratory, Imperial College, London SW7 2AZ, United Kingdom*
[3]*Laboratory for Laser Energetics, University of Rochester, Rochester, NY 14623, USA*
[4]*Los Alamos National Laboratory, Los Alamos, NM 87545, USA*

Low-mode asymmetries have emerged as one of the primary challenges to achieving high-performing inertial confinement fusion implosions. These asymmetries seed flows in the implosions, which will manifest as modifications to the measured ion temperature (T_{ion}) as inferred from the broadening of primary neutron spectra. The effects are important to understand both to learn to control and mitigate low-mode asymmetries, and to experimentally more closely capture thermal T_{ion} used as input in implosion performance metric calculations. In this paper, results from and simulations of a set of experiments with a seeded mode 2 in the laser drive are described. The goal of this intentionally asymmetrically driven experiment was to test our capability to predict and measure the signatures of flows seeded by the low-mode asymmetry. The results from these experiments (first discussed in M Gatu Johnson et al, Phys. Rev. E **98**, 051201(R) (2018)) demonstrate the importance of interplay of flows seeded by various asymmetry seeds. In particular, measured T_{ion} and self-emission x-ray asymmetries are expected to be well captured by interplay between flow seeded by the imposed mode 2 and the capsule stalk mount. Measurements of areal density asymmetry also indicate the importance of the stalk mount as an asymmetry seed in these implosions. The simulations brought to bear on the problem (1D LILAC, 2D xRAGE, 3D ASTER and 3D Chimera) show how thermal T_{ion} is expected to be significantly lower than T_{ion} as inferred from the broadening of measured neutron spectra. They also show that the electron temperature is not expected to be the same as T_{ion} for these implosions.

I. INTRODUCTION

Inertial confinement fusion aims to achieve ignition and burn through laser-driven symmetric compression of cryogenically layered capsules of deuterium-tritium (DT) fuel.[1] This can be done using either indirect drive[2,3], where the laser beams are incident on the inner walls of a hohlraum, generating x-rays which subsequently drive the capsule implosion, or direct drive[4,5], with the laser beams directly incident on the capsule. Independent of approach, low-mode asymmetries have emerged as a primary challenge to achieving ignition.[2,3,4,6,7,8,9,10,11,12] Low-mode asymmetries seed flows in the assembled fuel.[6,8] Ion temperature (T_{ion}) from inertial confinement fusion is traditionally inferred from the broadening of energy spectra of neutrons generated in the DT fusion reactions.[13,14] Flows seeded by low-mode asymmetries will manifest as modifications to the emitted neutron spectra and inferred apparent T_{ion}.[15,16] Uniform radial or turbulent flows will result in an overall enhancement in inferred T_{ion}, while asymmetric flows will lead to line-of-sight (LOS) variations in T_{ion}.[17] For this reason, measurements of the neutron spectra from various angles around an ICF implosion can be used to infer properties of the flow field in the implosion.

Ultimately, accurate diagnosis of the implosion flow field should allow for unambiguous identification of the factors seeding the flows, which is a prerequisite for controlling the low mode asymmetries and improving the implosions. Controlled vortex flows have even been proposed as a path to improved implosions,[18] but such a platform obviously requires a detailed understanding of how to initiate and characterize the flows. Additionally, improved understanding of the impact of flow on T_{ion} as inferred from measured neutron spectra is also important as T_{ion} is used as input to calculations of the pressure metric used to gauge implosion performance on the road to ignition.[4,19,20] This paper describes a set of direct-drive OMEGA[21] experiments explicitly designed to test our ability to accurately predict and characterize the impact of low mode asymmetries on the implosion flow field. Previous experiments have also involved intentionally asymmetrically driven OMEGA implosions (see e.g. Refs. 22,23,24,25), but inference of the impact of these asymmetries on the implosion flow field and directional inferred apparent T_{ion} has not previously been attempted. In the experiments discussed in this paper, a mode 2 asymmetry was intentionally imposed by reducing the laser drive in two opposing cones around the implosion, and apparent T_{ion} measured at angles parallel and perpendicular to the imposed asymmetry. Comparison of the results from these experiments with 3D simulations not including the capsule stalk mount lead to the conclusion that interplay between flows arising due to different asymmetry seeds impact the diagnostic signatures. In particular, interplay between the imposed mode 2 asymmetry in the laser drive and the intrinsic asymmetry seeded by the capsule stalk mount appears to describe the results well, as discussed in Ref. 26. In the present paper, the results from measurements and simulations of this asymmetry experiment are discussed in more detail, supporting the conclusion from Ref. 26 and describing many additional more subtle insights not possible to convey in the limited letter format.

The paper is organized as follows. Sec. II describes experiment setup and main results, and Sec. III discusses the simulation tools brought to bear to interpret the results from the implosions. In Sec. IV, measured and simulated observables are compared, and the implications of the comparisons are discussed. Sec. V concludes the paper.

II. EXPERIMENT

Five implosions were executed as part of this experiment: one symmetric reference implosion with nominally 450 J energy/beam, and two implosions each with the mode 2 asymmetry aligned along two different axes. All implosions used 860-μm outer diameter, 15-μm thick CH shell capsules filled with DT^{3}He gas (FIG. 1a). The asymmetries were designed to maximize the observable signatures in the LOS of the OMEGA DT neutron spectrometers operating at the time of the experiment: a scintillator-based detector 12m from the implosion at polar, azimuthal angles θ,φ=87.9°,161.2° (12mntof), a scintillator-based detector 15.8m from the implosion at θ,φ=61.3°,47.6° (15.8mntof) and a CVD-diamond based detector 5m from the implosion at θ,φ=85.0°,311.8° (5.0mcvd).[27,28,29] FIG. 1 shows the nominal imposed drive asymmetries as simulated using the VisRad code[30]. The first asymmetry, henceforth denoted Asym. A (FIG. 1b), was designed with the energy reduced to 315 J in 10 beams each of two opposing cones nearly aligned with the 15.8mntof LOS, and nearly perpendicular to the 12mntof and 5.0mcvd LOS. The second asymmetry, henceforth denoted Asym. B (FIG. 1c), was designed to "flip" the asymmetry relative to Asym. A for maximum diagnostic signatures, with the two opposing reduced-energy cones nearly aligned with the 5.0mcvd and 12mntof LOS, and nearly perpendicular to the 15.8mntof LOS. Because of the OMEGA 60-beam port geometry, the energy had to be reduced in 12 beams in each cone for Asym. B (with 6 beams reduced to 371 J and 6 to 304 J) to achieve an asymmetry equivalent to Asym. A.

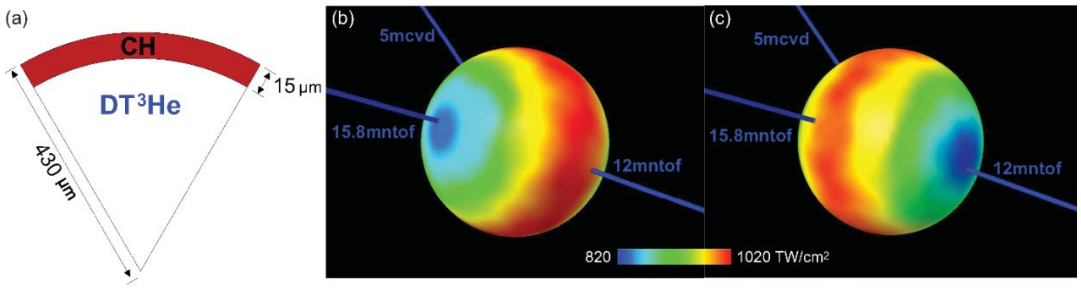


FIG. 1. Nominal experiment geometry. (a) 15-µm thick CH shell capsules filled with 12 atm DT gas and 6 atm ^{3}He gas were used in the experiment. (b,c) Mode 2 laser drive asymmetries were imposed in two different directions, Asym. A and Asym. B. Panels (b) Asym. A and (c) Asym. B show the asymmetries from the same viewing angle (θ=60°, ϕ=110°) as simulated using VisRad. The viewing directions of the three primary nTOF detectors relative to the imposed asymmetries are also indicated.

Table I. Laser and target parameters for the five individual implosions performed as part of this experiment. Note that in addition to the CH shell thickness, there is also a 0.1µm Al coating to prevent leakage.

Shot	Symmetry	Laser energy (kJ)	Outer diameter (µm)	CH shell thickness (µm)	4πΔ wall (µm)	Glue spot diameter (µm)	Glue spot length (µm)	DT fill (atm)	^{3}He fill (atm)
79358	Sym. ref.	25.7	872	14.4	0.2	77.05	98.12	11.0	6.9
79359	Asym. A	22.7	872	14.5	0.4	83.15	97.56	12.4	7.8
79362	Asym. B	23.2	873	14.5	0.2	61.53	85.37	12.3	7.8
79363	Asym. A	23.2	870	14.3	0.2	56.54	80.93	12.0	7.6
79364	Asym. B	23.5	875	14.2	0.1	61.53	79.82	11.8	7.5

Capsule and laser parameters for all five implosions are summarized in Table I. Here, the "4πΔ wall" number represents a measurement of variation in shell thickness around the targets; as can be seen, the capsules were measured to be very uniform with 4πΔ wall ≤ 0.4 for all implosions. The capsules were held at target chamber center (TCC) with the TPS2 target positioner at θ,φ=37.4°,90.0°, using 17-µm diameter SiC stalks attached with a glue spot. They were imploded using all 60 available OMEGA laser beams with a 1-ns square laser pulse shape, with distributed phase plates, and with two-dimensional smoothing by spectral dispersion[31] and polarization smoothing[32] applied. Under these conditions, on-target illumination non-uniformity better than 2% rms[33] is expected without any external perturbations applied. However, previous work has shown that a number of external asymmetry seeds, including unintended drive asymmetry,[11] unintended capsule misalignment (offset),[9,34] and the capsule stalk mount[35,36,37] can be expected to modify this picture. The anticipated effect of these factors is illustrated in FIG. 2, which shows the VisRad-simulated laser intensity for Asym. A shot 79359 as a function of polar and azimuthal angles. The three plus signs in each panel represent the locations of the three nTOF detectors, from left to right 15.8mntof, 12mntof and 5.0mcvd; the star represents the location of the stalk mount. FIG. 2a shows the nominal (requested) mode 2 drive asymmetry. The as-shot laser drive is characterized on each OMEGA implosion, with measurements of both energy (using the harmonic energy detector) and timing (using the P510 streak cameras) of each beam.[38,39] These measurements come with the caveat that they are made outside of the target chamber, and have to be corrected for transmission through the final optics assembly/blast shield windows on the way to TCC. However, the experiments described here were executed two days after blast shield replacements, which means the beam energy balance measurements are expected to be accurate. FIG. 2b shows the measured, as-shot laser drive for shot 79359. The small differences seen compared to the nominal drive in FIG. 2a are captured in post-shot simulations, which include the measured, as-shot drive. As-shot capsule offsets are inferred from images recorded using a system of five x-ray pinhole

cameras.[40] For shot 79359, the offset was determined to be 16μm in the direction θ,φ=152°,4°. Considering both the capsule offset and the as-shot laser drive in the VisRad simulation of on-target laser intensity gives the result shown in FIG. 2c. Again, some differences can be seen compared to the nominal drive in FIG. 2a, but they are not large enough to significantly impact the experiment as will be shown below. The final obvious additional factor to impact the drive is the stalk mount. This is not as easily captured in VisRad simulations. FIG. 2d shows the result of a VisRad simulation including the glue spot and as-shot drive but not the capsule offset. Unfortunately, the only thing this simulation really shows is the anticipated weak spot in the drive under the glue spot itself. The impact of this on the implosion cannot be determined based on this simplified picture.

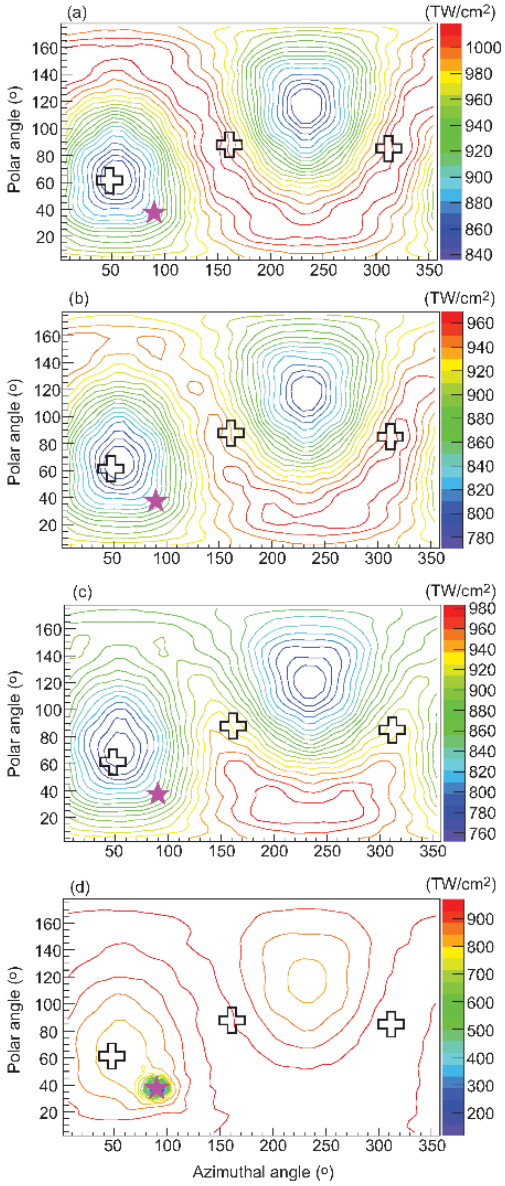


FIG. 2. Laser intensity versus polar and azimuthal angle for shot 79359 as simulated using VisRad, (a) with the nominal drive, (b) with as-shot drive asymmetry, (c) including measured as-shot offset, and (d) including stalk and glue spot but not including offset. The three plus signs represent the locations of the three nTOF detectors, from left to right 15.8mntof, 12mntof and 5.0mcvd, and the star represents the location of the stalk mount.

The implosion intended as a symmetric reference will also be impacted by these effects. FIG. 3 shows the VisRad-simulated laser intensity plot for symmetric reference shot 79358, considering the measured as-shot laser drive and capsule offset (for this implosion, the measured offset was 8.5μm in the θ,φ=93°,355° direction). There is an apparent mode 1 of about 6% peak-to-valley in this implosion, to be compared to the 29% mode 2 seen in the equivalent plot for shot 79359 in FIG. 2c. The hollow star in FIG. 3 indicates the direction of the offset. The fact that the mode 1 is not in the direction of the offset suggests that the intrinsic mode 1 drive asymmetry has a stronger impact on this implosion than the offset does.

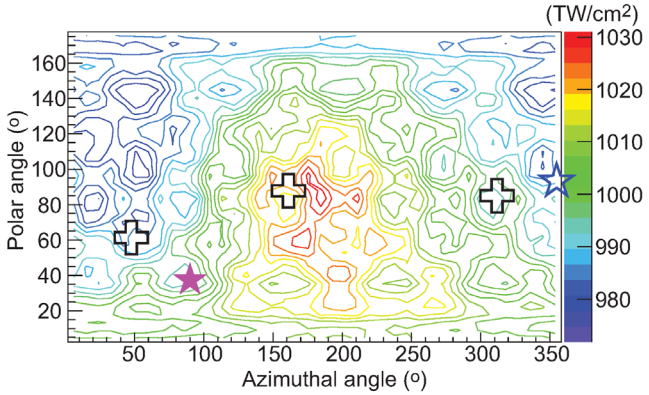


FIG. 3. VisRad-simulated laser intensity distribution considering measured capsule offset and as-shot drive for symmetric reference implosion 79358. The three plus signs represent the locations of the three nTOF detectors, from left to right 15.8mntof, 12mntof and 5.0mcvd, the solid star represents the location of the stalk mount and the hollow star the direction of the offset.

FIG. 4 shows the VisRad-simulated laser intensity distributions considering offset and as-shot asymmetry for the four intentionally asymmetrically driven implosions. FIG. 4a,c represent the Asym. A implosions, while the Asym. B implosions are illustrated in panels b,d. The hollow blue stars represent the direction of the offset for each implosion; offset magnitudes were determined to be 16μm for shot 79359, 10μm for shot 79362, 16μm for shot 79363 and 16μm for shot 79364. Note that the offset directions are very similar for the two Asym. B implosions (FIG. 4b,d), which leads to near identical intensity distributions for these two shots. For the two Asym. A implosions (FIG. 4a,c), the offset directions are more different, which manifests as slightly more visible differences in the intensity distributions in this case.

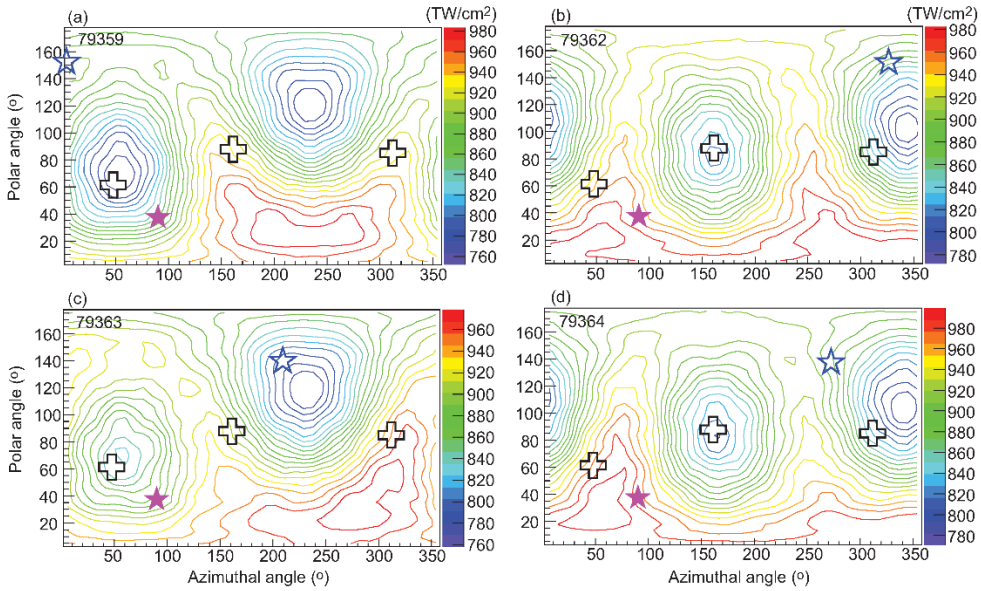


FIG. 4. VisRad-simulated laser intensity distribution considering measured capsule offset and as-shot drive for Asym. A shots 79359 (a) and 79363 (c), and for Asym. B shots 79362 (b) and 79364 (d). The three plus signs represent the locations of the three nTOF detectors, from left to right 15.8mntof, 12mntof and 5.0mcvd, the solid star represents the location of the stalk mount and the hollow star the direction of the offset. The plots demonstrate that the as-shot asymmetry for the two Asym. B shots (79362, 79364) are much more similar than the as-shot asymmetry for the two Asym. A shots (79359, 79363).

FIG. 5 shows T_{ion} measured using the 12mntof, 15.8mntof and 5.0mcvd detectors, with the symmetric reference implosion (green diamonds) contrasted to the two Asym. A implosions in panel (a) and the two Asym. B implosions in panel (b). The first thing to note is that an apparent T_{ion} asymmetry is observed for the symmetric shot, with a higher measured T_{ion} in the 12mntof LOS. It cannot be ruled out that this apparent difference is a detector-to-detector calibration issue. Since the three nTOF detectors are routinely recalibrated against each other on warm implosions such as these, if there was a systematic difference due to e.g. stalk effect, it would be calibrated out (warm implosions are almost always held by the same TPS2 target positioner using similar mounts). For this reason, when we look at the asymmetrically driven implosions, we chose to study these in relation to the symmetric reference. The second thing to note in FIG. 5 is that the T_{ion} results for the Asym. A implosions are incredibly consistent between the two shots (79359 and 79363), while for the Asym. B implosions, there are much larger variations between the two shots (79362 and 79364). This is in contrast to the more similar as-shot drives for the two Asym. B implosions compared to for the two Asym. A implosions (FIG. 4), indicating that the small differences in as-shot drive due to the capsule offsets do not significantly affect our results. It is also in contrast to the larger "4πΔ wall" variations between the two Asym. A than between the two Asym. B capsules (Table I), also indicating that the small variations in wall thickness around the capsules do not significantly impact the observations. For Asym. A, the stalk is at 37° to the asymmetry axis, while for Asym. B, the stalk is at 71° to the asymmetry axis. We conjecture that the lesser consistency for two Asym. B implosions is likely a result of jetting from the stalk mount interfering with the seeded mode 2 asymmetry in this case, making the flow field harder to predict. For Asym. A, a consistent enhancement in measured T_{ion} relative to the symmetric implosion is seen for the 15.8mntof detector, which is located nearly parallel to the imposed mode 2 asymmetry. For Asym. B, an overall increase in apparent T_{ion} is observed relative to the symmetric shot. The overall increase in average T_{ion} on all asymmetric shots, which is seen in spite of the 10% lower total laser energy on these

implosions relative to the symmetric case, demonstrates that enhanced flow was achieved in these implosions as intended. The results are contrasted to simulation in Sec. IV.

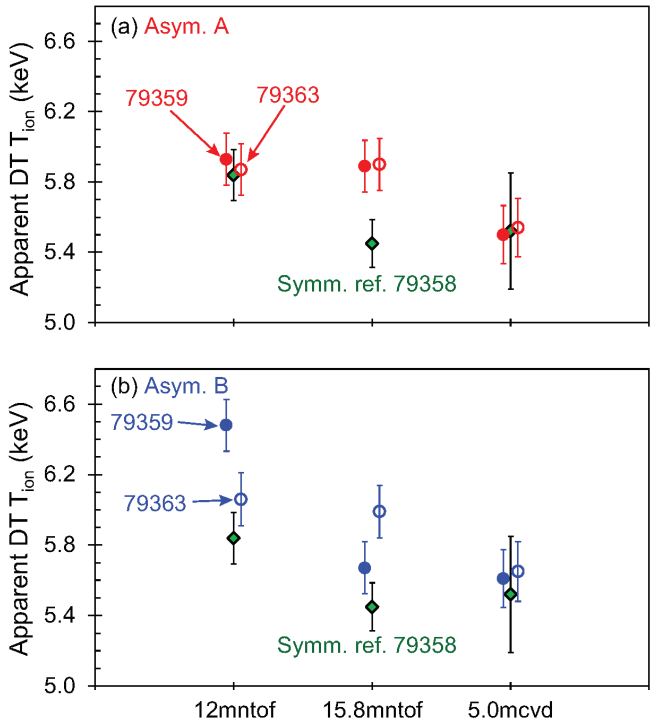


FIG. 5. Measured T_{ion} on (a) the two Asym. A shots (red circles) contrasted to the symmetric reference (green diamonds) and (b) the two Asym. B shots (blue circles) contrasted to the symmetric reference (green diamonds).

Table II lists the DT neutron yields on these implosions as measured with the 12mntof, 15.8mntof and 5.0mcvd neutron spectrometers. The precision quoted in the yield measurement from each detector is better than 1%, but the measurements from the three are different by ~5%. We take the yield to be the average of the three measurements and the uncertainty to be the standard deviation. An average DT yield reduction of 36% is observed between the symmetric and asymmetric implosions. A carefully balanced mix of D/T/^{3}He fuel was used in these experiments to allow simultaneous measurements of DT-neutron and D^{3}He-proton yields. Table II also lists the D^{3}He-proton yields inferred from Wedge Range Filter (WRF)[41] proton spectrometers in TIM4 with θ,φ=63.4°,342.0° and P2NDI with θ,φ=57.6°, 54.0°, and from MRS[42] with θ,φ=119.3°,308.0°, CPS1[43] with θ,φ=63.4°,198.0° and CPS2 with θ,φ=37.4°,18.0°. Again, the standard deviation between the five measurements is taken as the uncertainty. The average yield reduction observed for the D^{3}He reaction between the symmetric and asymmetric shots is 46%.

Table II. Measured DT-neutron and D^{3}He-proton yields. The DT neutron yield is the average between three nTOF LOS, and the D^{3}He proton yield the average between five proton spectrometer LOS. The quoted uncertainties represent the standard deviation of the individual measurements.

Shot	Type	DT-n yield (×10^{12})	D^{3}He-p yield (×10^9)
79358	Symmetric	11.6 ± 0.3	5.4 ± 1.6
79359	Asymm #1 (P2-P11)	5.5 ± 0.3	2.5 ± 0.4
79362	Asymm #2 (H8-H13)	6.5 ± 0.4	2.2 ± 0.6
79363	Asymm #1 (P2-P11)	8.6 ± 0.3	3.3 ± 1.2
79364	Asymm #2 (H8-H13)	8.9 ± 0.2	3.8 ± 0.6

As discussed in the introduction, T_{ion} inferred from the broadening of primary neutron spectra will always be impacted by any residual flows in the implosion at burn. An alternative, flow-independent way of inferring T_{ion} is the yield ratio method,[44] where T_{ion} is determined from the relative yields of two reactions whose reactivities have different T_{ion} dependence. T_{ion} inferred from this method, using the yields from Table II, reactivity parametrizations from Ref. 45 and neglecting profile effects, are contrasted to nTOF-measured T_{ion} in FIG. 6. Unfortunately, the yield ratio method T_{ion} error bars, which are dominated by the uncertainty in the D^3He-proton yield measurement, are too large to meaningfully contribute any additional information on the impact of flow.

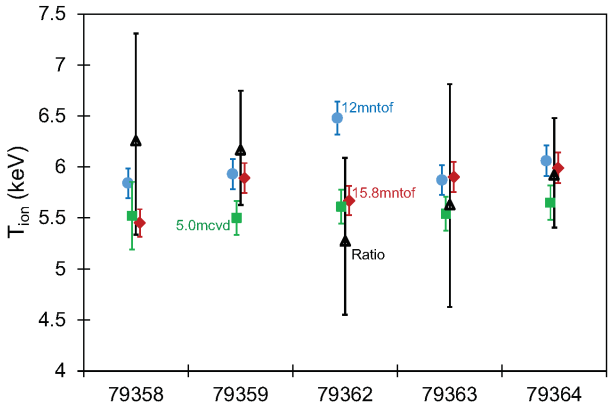


FIG. 6. T_{ion} inferred using ratio method (black triangles) compared to T_{ion} as measured using the nTOF detectors (blue circles for 12mntof, red diamonds for 15.8mntof and green squares for 5.0mcvd). Note the much larger uncertainty in the ratio method T_{ion}, which is primarily driven by the uncertainty in the D^3He-p yield measurement.

Each of the five proton spectrometers measures the proton energy spectrum. As an example, the CPS1-measured proton spectrum from Asym. A shot 79363 is shown in FIG. 7. Because of the D/T/^{3}He gas-fill and the CH shell, there are two components to the spectra: knock-on protons (KO-p) from DT-neutrons elastically scattering on protons in the shell, and D^3He protons. The spectra are analyzed using a Gaussian to describe the D^3He peak and an MCNPX-simulated[46] component to describe the KO-p continuum. In addition to the D^3He yield, the D^3He proton energy downshift and the KO-p yield are also determined from the data. These latter two quantities are used to infer the areal density (ρR) of the implosions, with the total areal density (fuel and shell) inferred from the energy downshift[47], and the shell areal density inferred from the ratio of KO-p yield to primary DT neutron yield[48]. Total ρR inferred from all measured proton spectra are listed in Table III. These numbers are inferred from the measured D^3He-p mean energy using 1D-simulated profiles of the implosion to correlate downshift to ρR as calculated from the center of the implosion. Also included in Table III is the angle between each proton spectrometer and the stalk that holds the target. As can be seen, the inferred ρR is consistently low for the P2NDI line-of-sight, which is closest to the stalk. This is expected from simulations, as is further discussed in Sec. IV below (FIG. 22). Sec. IV also includes discussion of how the drive asymmetry manifests in the ρR measurements (in the context of FIG. 23).

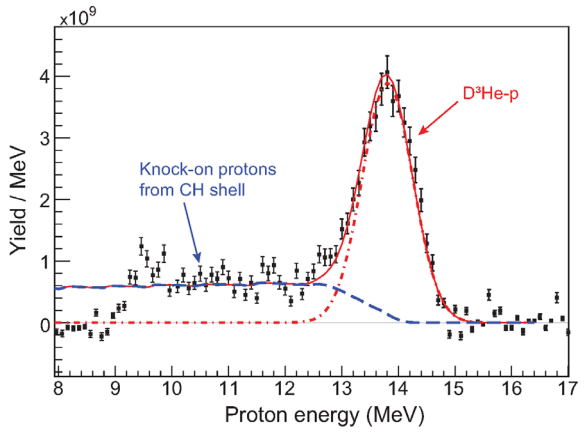


FIG. 7. Example proton spectrum showing how ρR was measured. This is the CPS1 data from shot 79363. There is a detector cut-off at ~9.5 MeV. The peak at 13.8 MeV is the D^3He protons, while the continuum towards lower energies is knock-on protons (KO-p) from elastic scattering of DT neutrons in the CH shell. The two-component fit (total fit solid red curve, KO-p dashed blue curve, and D^3He-p broken red curve) is limited to E_p>11 MeV.

Table III. Total areal density (ρR) in five different LOS as inferred from measured D^3He-proton energy downshift compared to the nominal D^3He-p birth energy of 14.7 MeV.

	Total ρR (mg/cm^2)					
Shot	79358	79359	79362	79363	79364	Angle to stalk
TIM4	35.9±3.3	40.3±3.5	33.9±2.5	38.3±3.6	27.8±3.0	79.2°
P2NDI	28.5±3.6	29.0±3.0	30.1±3.6	28.5±2.5	30.8±3.6	32.8°
MRS	42.3±5.6	44.0±5.6	29.3±5.5	33.7±5.5	27.7±5.5	143.7°
CPS1	31.4±7.4	35.9±7.0	31.8±8.4	28.4±6.9	39.3±8.1	79.2°
CPS2	42.6±7.1	38.1±8.5	40.2±7.0	45.1±9.1	34.5±7.2	41.8°

In addition to the nuclear data, self-emission x-ray images as a function of time were also recorded on two of these implosions (79363 and 79364) using a framing camera located at θ,φ=37.4°,162.0°. With this fixed viewing angle, the camera is expected to see 98% of the imposed Asym. A and 67% of the imposed Asym. B. Two example images from Asym. A implosion 79363 are shown in FIG. 8. Implosion size as well as the magnitude of the mode 2 asymmetry are inferred from these images using the method described in Ref. 49. The results are contrasted to numbers inferred from simulated synthetic x-ray images in Sec. IV below (FIG. 20).

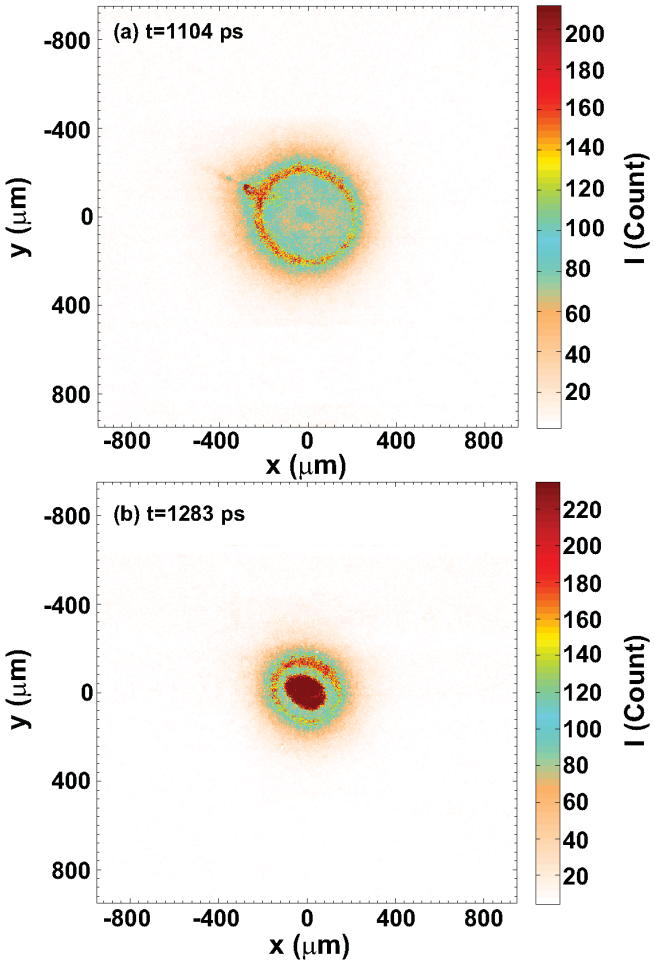


FIG. 8. Example self-emission x-ray images taken at t=1104 ps (a) and t=1283 ps (b) for shot 79363. The framing camera used to record the images is located at θ,φ=37.4°,162.0° and is expected to see 98% of the imposed asymmetry for this Asym. A implosion. Note that the ellipticity can be seen to grow with time – a mode 2 of 4.0% is inferred for the image in (a), and a mode 2 of 9.6% is inferred for the image in (b). Size and ellipticity results as a function of time inferred from images of this type are contrasted to simulations in FIG. 20 below.

Backscattered laser light was measured on these implosions using time-resolved full-aperture backscatter calorimetry.[50] The absorbed laser light fractions inferred from these data (listed in Table IV) are used to constrain simulations. For spherical shots, the scattered light at any point in the target chamber is a superposition of scattered light from all 60 beams, and the absorption measurements are not expected to be particularly affected by the lower intensity in some of the beams for the asymmetric implosions.

Table IV. Absorbed laser light fractions as inferred from scattered light measurements.

Shot	Absorbed laser light
79358	55 +/- 2%
79359	61 +/- 4%
79362	60 +/- 8%
79363	61 +/- 1%
79364	60 +/- 10%

III. SIMULATIONS

Several different simulation tools were brought to bear on these experiments to interpret the results. These include 1D LILAC[51], 1D and 2D xRAGE[36,52,53] 3D ASTER[9,10] and 3D Chimera[54], with the latter initialized with 1D HYADES[55]. Results from each are briefly discussed below.

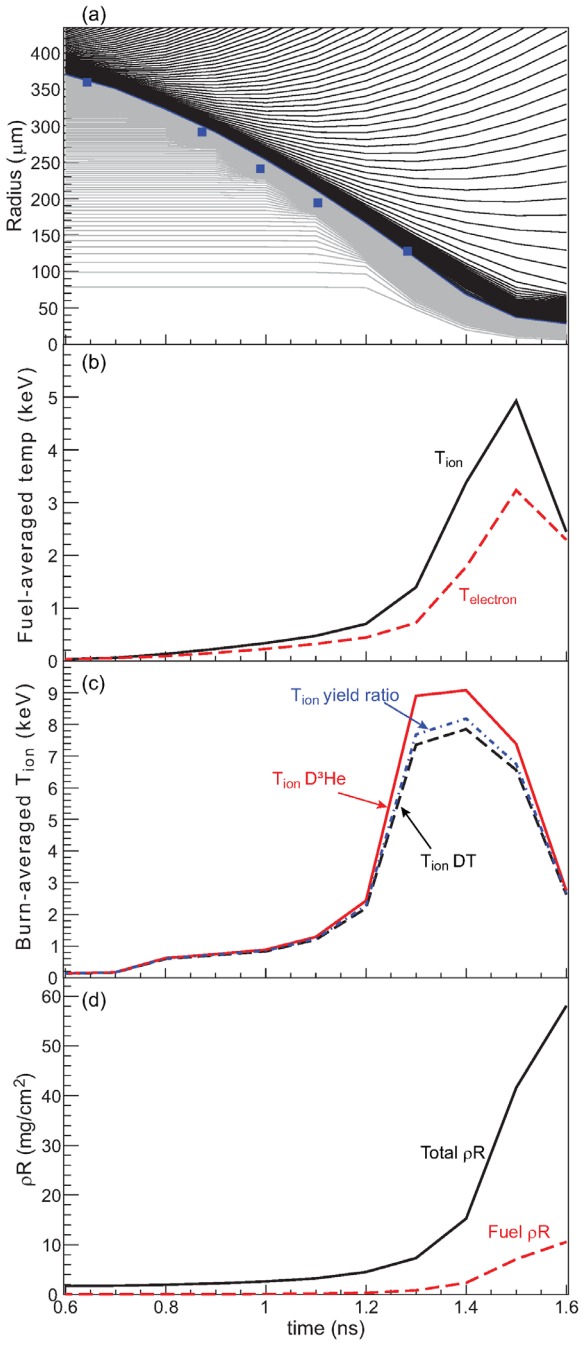


FIG. 9. 1D LILAC simulations of shot 79363. (a) Lagrangian radius versus time plot where gray curves represent the time evolution of fuel elements, black the time evolution of shell elements, and the thick blue curve the fuel-shell interface trajectory. Also shown is the fuel-shell interface inferred from self-emission x-ray imaging on shot 79363 (blue squares). (b) Fuel-averaged T_{ion} (solid black) and $T_{electron}$ (dashed red) history, (c) D^3He (solid red) and DT (dashed black) burn-averaged T_{ion} and T_{ion} inferred from the simulation using the ratio method (broken blue), and (d) total (solid black) and fuel (dashed red) ρR. Burn-averaged total ρR is 38.9 mg/cm^2, fuel ρR 6.6 mg/cm^2.

1D LILAC

LILAC[51] is an extensively benchmarked 1D Langrangian radiation-hydrodynamics code routinely used to simulate direct-drive OMEGA implosions. Because it is 1D, it cannot consider imposed low-mode asymmetries. However, it was used to give a baseline 1D comparison simulation of implosion 79363. The results are summarized in FIG. 9. Panel (a) shows the Lagrangian radius versus time plot illustrating the overall time evolution of the implosion, with the solid blue line representing the fuel-shell interface. Also shown for comparison is the measured fuel-shell interface as a function of time inferred from self-emission x-ray imaging (blue squares); the LILAC simulation is seen to capture the overall dynamics of the implosion very well. Panel (b) shows the fuel-averaged T_{ion} and electron temperature ($T_{electron}$), panel (c) burn-averaged DT, D^3He and ratio T_{ion}, and panel (d) total and shell ρR, all as a function of time. FIG. 10 shows the instantaneous LILAC-simulated radial T_{ion}, $T_{electron}$ and density (ρ) profiles at the simulated bang time (1.5 ns, panel a) and shortly after burn (1.6 ns, panel b). The fuel-averaged T_{ion} and $T_{electron}$ in FIG. 9b represent a straight average over all radial elements in the fuel (but excluding shell elements). The burn-averaged T_{ion} in FIG. 9c, on the other hand, is weighted by the expected yield (Y) as a function of radius, with $Y \sim \rho^2 \times \langle \sigma v(T_{ion}) \rangle \times$volume. Note that these numbers represent expected thermal T_{ion} and do not consider any impact of flow.

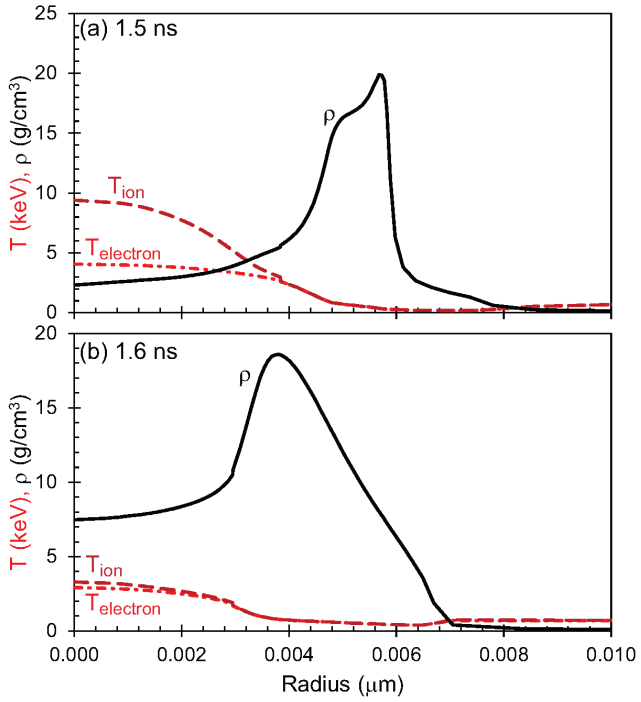


FIG. 10. Radial profiles at (a) t=1.5 ns (simulated bang time) and (b) t=1.6 ns from the LILAC simulation shown in FIG. 9. Solid black curves represent density, dashed maroon curves T_{ion}, broken red curves $T_{electron}$.

The first important observation to be made here is that T_{ion} and $T_{electron}$ are not expected to be the same for these experiments; as can be seen from FIG. 9b, T_{ion} grows faster than $T_{electron}$ and the equilibration time is long on the time scale of the implosion. This is interesting as measurements of $T_{electron}$ have been proposed as an alternative to T_{ion} measurements in an attempt to circumvent the flow problem and get a measurement of the thermal T_{ion} needed as input for calculating the pressure performance metric frequently used to gauge progress towards ignition.[4,19,20] While T_{ion} and $T_{electron}$ are expected to be more similar for cryogenically layered implosions than for the shots studied here, any attempts to infer thermal T_{ion} from measured $T_{electron}$ must consider expected differences between these two quantities.

The second important observation to be made based on the LILAC results is that we do not expect DT, D^3He and ratio T_{ion} to give identical answers even in the absence of flows. The differences seen between these three quantities in FIG. 9c arise simply due to radial profile/reactivity effects.

3D Chimera

The most extensive post-shot simulations of this experiment have been done using the Eulerian-mesh 3D Chimera code[54]. Chimera is initialized with 1D HYADES simulations after laser turn-off but before the shock hits the center. A number of HYADES simulations with varying laser powers are used to mock-up the as-shot drive asymmetry; drive powers are adjusted to match the average measured absorbed energies (Table IV). Importantly, the simulations do not consider the capsule stalk mount. The actual locations of the nTOF detectors and the x-ray framing camera are considered when generating synthetic diagnostic results from the simulations. Full neutron spectra are calculated for each nTOF LOS, and a synthetic "T_{ion}" inferred by fitting a Gaussian to these neutron spectra.

A "no-flow", thermal T_{ion} is also easily calculated from the simulation by neglecting flow broadening contributions to the neutron spectra. Average, minimum and no-flow Chimera-simulated T_{ion} from post-shot simulations of the five implosions are summarized in FIG. 11. Note that for the symmetric reference shot, minimum and average T_{ion} are nearly identical, but both are higher than the no-flow T_{ion} by about 0.4 keV. For the asymmetrically driven implosions, the difference between thermal and minimum T_{ion} is even larger, ranging from 0.7-0.8 keV. This is an important observation - minimum T_{ion} has been frequently used in calculations of implosion pressure[4,56] because it is assumed to be closest to thermal, but we see that even minimum T_{ion} is unlikely to be a good representation of the thermal T_{ion}.

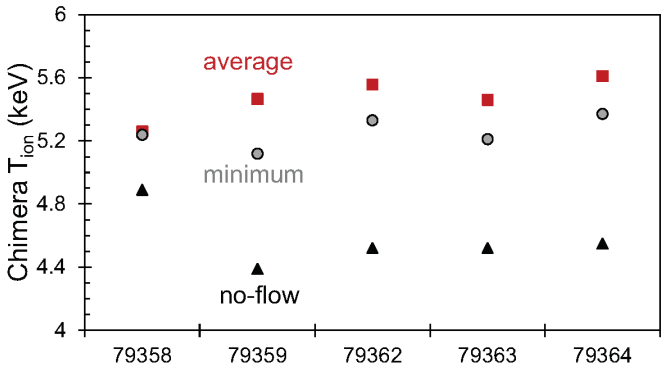


FIG. 11. Average, minimum and thermal (no-flow) T_{ion} simulated using 3D Chimera for each of the five implosions studied for this paper.

FIG. 12 shows the Chimera-simulated time evolution of inferred T_{ion} for Asym. A shot 79359. For this implosion, the 5.0mcvd, 12mntof and TIM6 (which was not used in the experiment) detectors are all located roughly perpendicular to the imposed asymmetry, while the 15.8mntof detector is located nearly parallel to the asymmetry. We see that early on, when the implosion is still compressing along all axes, a higher apparent T_{ion} is expected to be observed for the detectors perpendicular to the asymmetry. This is consistent with the laser pushing harder on the implosion here, introducing a faster fuel flow. The simulated burn pulse is also plotted in FIG. 12 (right axis). As can be seen, shortly before peak burn the T_{ion} asymmetry flips, with higher apparent T_{ion} now expected parallel to the imposed asymmetry. The cross-over point represents the time when outflow starts along the asymmetry axis. According to the Chimera simulations, most of the implosion yield is generated after the cross-over point, leading to maximum time-integrated T_{ion} observed parallel to the imposed asymmetry. However, this plot clearly emphasizes how challenging it is to predict

the impact of the mode 2 on implosion observables. A slight change in the relative timing of burn and outflow along the asymmetry axis could flip the asymmetry and give maximum T_{ion} perpendicular rather than parallel to the imposed mode 2. Such a timing change could e.g. result from burn truncation, which could arise due to e.g. mix caused by high-mode asymmetries or stalk jetting.

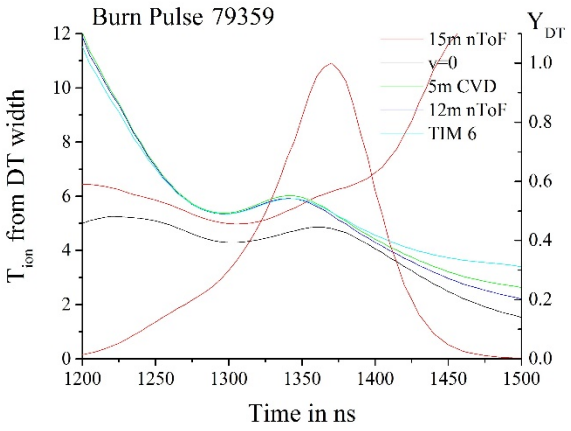


FIG. 12. Chimera-simulated T_{ion} versus time for shot 79359. The black (lowest) curve represents the no-flow T_{ion}. The 5.0mcvd (green), 12mntof (blue) and TIM6 (cyan; not used in the experiment) detectors are all located approximately perpendicular to the imposed drive asymmetry for shot 79359, while 15.8mntof (red) is located parallel to the imposed asymmetry. The simulated burn pulse is shown in red (right scale). The T_{ion} asymmetry flips during the burn pulse for this mode 2 experiment – early in the implosion, the detectors perpendicular to the asymmetry see the highest apparent T_{ion}, while late in the burn pulse, the detector parallel to the asymmetry sees the highest apparent T_{ion}. The cross-over happens when outflow starts along the asymmetry axis.

Comparing Chimera simulations considering only the nominal, requested laser drive to the final simulations using the as-shot drive demonstrate that the as-shot drive gives a substantially reduced T_{ion} asymmetry compared to the nominal drive, by of order 1 keV. This is because the intrinsic asymmetry in the drive interferes with the axial symmetry of the mode 2 and reduces the coherence of the outflow along the asymmetry axis. We also note that running Chimera with multimode asymmetries in addition to the imposed mode 2 leads to an overall increase in apparent T_{ion} (due to additional overall flow broadening), but does not eliminate the T_{ion} anisotropy.

Chimera-simulated yields and T_{ion} are summarized in Table V. The Chimera simulations do not have ^{3}He added in the fuel, but the yield numbers in the table have been corrected to account for this based on empirical observations of a factor 2 reduction in yield between 50:50 D:T implosions (average DT yield 2.4×10^{13} for reference shots 70871, 70878 and 70879) and our symmetric D:T:^{3}He reference (1.2×10^{13} yield) (the raw simulated yields were multiplied by 0.5 to give the values in Table V).

Table V. Chimera-simulated yields and T_{ion} for each LOS for each of the five implosions studied here. Also shown is the thermal "no-flow" T_{ion} (v=0), which is inferred if broadening due to flow is eliminated from the simulated neutron spectra. Note that Chimera does not include ^{3}He in the fuel. The simulated yields have been adjusted to account for this.

	Yield	T_{ion} (keV)			
Shot	($\times 10^{13}$)	v=0	5.0mcvd	15.8mntof	12mntof
79358	3.45	4.89	5.28	5.24	5.26
79359	1.61	4.39	5.24	6.04	5.12
79362	1.94	4.52	5.61	5.33	5.73
79363	1.92	4.52	5.31	5.86	5.21
79364	1.99	4.55	5.67	5.37	5.79

3D ASTER

The 3D code ASTER, which has been previously used to model the impact of asymmetries on direct-drive OMEGA implosions,[4,9,10,11,57] has been used to model one of our implosions, 79363, with Asym. A imposed. ASTER is an Eulerian code optimized for direct drive implosions. It uses simplified models for heat transport and for 3D laser ray tracing. Like Chimera, it also does not include the capsule stalk mount. The post-shot simulation for 79363 implemented the measured, as-shot drive. The simulated absorption fraction was 60.2%, compared to measured 61±1%.

The ASTER simulations do see significant distortions due to the imposed mode 2 as expected. Contour plots of density and T_{ion} at peak neutron production (t=1.548 ns) are shown in FIG. 13. A clear ellipticity is seen with the points in the direction of the imposed asymmetry.

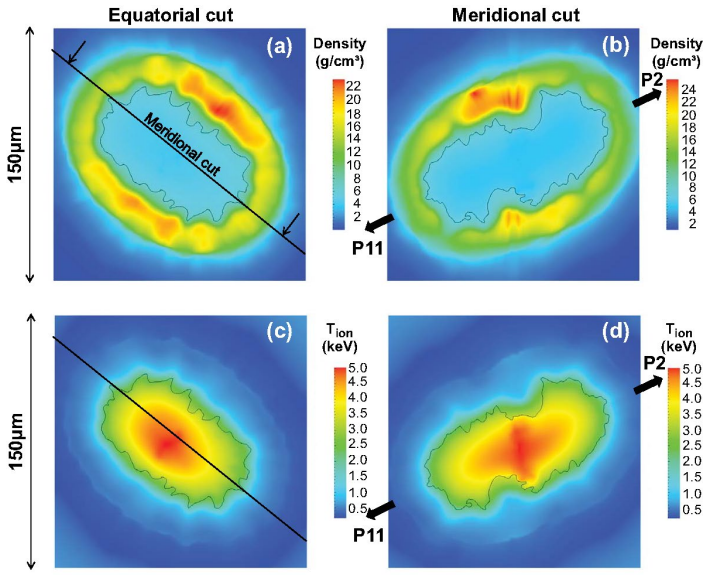


FIG. 13. Contour plots of (a,b) density and (c,d) T_{ion} at peak neutron emission from 3D ASTER simulations of shot 79363. (a,c) show an equatorial cross section, (b,d) a meridional cross section. The arrows shown in the meridional cut indicate the direction of the two OMEGA diagnostic ports (P2 and P11) at the center of each reduced-energy cone.

FIG. 14 shows the ASTER-simulated expected neutron spectra for shot 79363 in the 12mntof, 5.0mcvd and 15.8mntof LOS, along with the no-flow spectrum. Apparent T_{ion}=4.15 keV is inferred from the synthetic

12mntof and 5.0mcvd spectra perpendicular to the imposed mode 2, while T_{ion}=4.10 keV is inferred from the synthetic 15.8mntof spectrum, parallel to the imposed mode 2. This means the ASTER simulations show a minimal enhancement (50 eV) in apparent T_{ion} in the lines-of-sight *perpendicular* to the imposed asymmetry (in contrast to Chimera, which showed the T_{ion} enhancement parallel to the imposed asymmetry). A small overall enhancement in apparent T_{ion} (4.1 keV) compared to thermal T_{ion} (3.8 keV) is also seen. This level of enhancement is consistent with an overall average velocity (with random direction) of the burning fuel of 128 km/s. The ASTER-simulated yield comes in at 1.3×10^{13}. The ASTER simulation does include ^{3}He in the fuel.

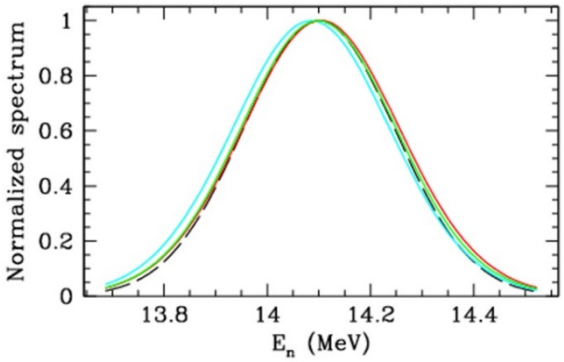


FIG. 14. Expected neutron spectra from ASTER. 12mntof (red, T_{ion}=4.15 keV), 15.8mntof (green, T_{ion}=4.10 keV) and 5.0mcvd (cyan, T_{ion}=4.15 keV) for shot 79363. Also shown is the neutron spectrum with no fuel flow considered (dashed black line, T_{ion}=3.82 keV).

1D/2D xRAGE

Unlike Chimera and ASTER, the Eulerian radiation hydrodynamics code xRAGE[52,53] does have the capability to simulate the impact of the capsule stalk mount.[36] xRAGE uses Adaptive Mesh Refinement (AMR). The use of Eulerian hydrodynamics with AMR makes xRAGE particularly well suited for modeling engineering features such as the stalk mount. xRAGE can be run in 1D, 2D or 3D mode, but as 3D simulations require extensive computational resources, only 1D and 2D simulations have been done for the implosions studied here. These simulations were performed with a maximum grid resolution of 0.25 μm, and in a similar fashion to those detailed in Ref. 36. Two types of 2D xRAGE simulations were run: (i) with the glue spot but excluding the imposed drive asymmetry, and (ii) with the as-shot drive but excluding the glue spot (the 2D geometry prevents simultaneous simulations of both asymmetry seeds). The xRAGE T_{ion} results are summarized in Table VI. Here, BWTI is the burn-weighted thermal, "no-flow" T_{ion} (note that BWTI is inferred from T_{ion} in each element of the simulation and not from fitting to the resulting neutron spectrum, in contrast to Chimera and ASTER-inferred thermal T_{ion}). The geometry is defined so that the asymmetry is aligned along the z axis (with z and –z being the parallel/antiparallel directions) and the x axis is perpendicular to the asymmetry. This means that LOS variations in T_{ion} are calculated directly parallel and perpendicular to the imposed asymmetry, and thus over-estimate what could actually be observed with the nTOFs, which are not perfectly orthogonal. The directional T_{ion}'s are inferred from the broadening of synthetic neutron spectra and do consider flows.

Table VI. T_{ion} inferred from 2D xRAGE simulations including either the glue spot (with no drive asymmetry) or the as-shot drive (with no glue spot). Because of the 2D geometry, both asymmetries cannot be simultaneously considered. BWTI is the "no-flow" T_{ion}, z and –z are the directions parallel and antiparallel to the imposed asymmetry and x the direction perpendicular to the asymmetry.

		T_{ion} (keV)				Average flow enhancement
Shot	Sim. type	BWTI	z	x	-z	(keV)
79358	Glue spot	5.27	6.29	6.27	6.19	0.98
79358	As-shot drive	5.66	6.18	6.24	6.18	0.54
79359	As-shot drive	4.83	4.99	5.14	4.99	0.21
79362	As-shot drive	5.42	6.11	6.11	6.12	0.69

We see from Table VI that LOS variations in T_{ion} due to the glue spot only (as simulated for the symmetric shot) are expected to be very small, only 0.1 keV. The as-shot drive asymmetry on the symmetric shot is expected to give a LOS variation in T_{ion} of 0.06 keV (pretty close to the Chimera prediction of 0.04 keV, Table V). Note that as the measured T_{ion} asymmetry will capture the interplay between the glue spot and drive asymmetry effects, the numbers cannot be directly compared with the measurement. However, we see that the order-of-magnitude variations expected from these effects are 0.1-0.2 keV, too small to be accurately captured outside of error bars with the nTOF detectors. For the imposed Asym. B (shot 79362), no LOS variation (0.01 keV) in T_{ion} is predicted; this is thought to be due to the inherent drive asymmetry counteracting the imposed asymmetry in this configuration. For the imposed Asym. A (shot 79359), the 2D simulations predict a LOS variation of 0.15 keV, with the enhancement expected perpendicular to the imposed asymmetry (consistent with ASTER, but in contrast to Chimera). Looking at FIG. 15, which shows the velocity field from the 2D drive asymmetry xRAGE simulations at bang time for shot 79359, we see that the reason for this is that burn in this simulation happens while the implosion is still compressing along all axes.

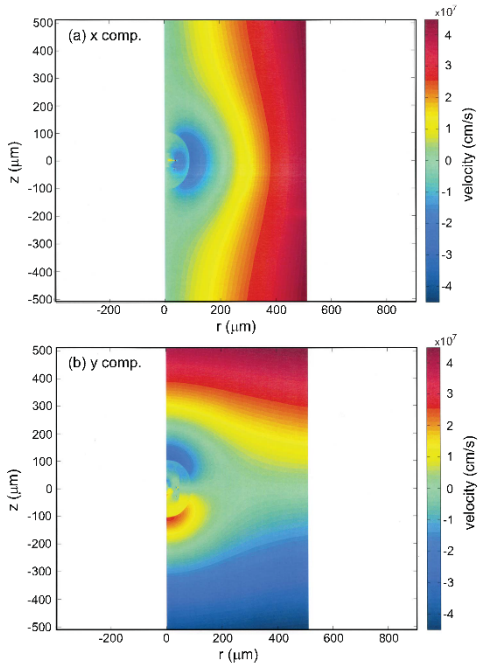


FIG. 15. Velocity field plots at bang time from 2D xRAGE simulations of shot 79359, showing (a) the x component and (b) the y component of the velocity as a function of radius r along the asymmetry axis z. These plots show that the xRAGE simulation is still compressing along all axes at the time of burn.

Interestingly, the simulation considering the glue spot only but not the as-shot drive shows an overall flow enhancement in inferred T_{ion} of nearly 1 keV. Combining this with the slightly lower expected enhancement due to as-shot drive gives expected measured T_{ion} significantly higher than thermal T_{ion}. The simulated flow enhancement over thermal T_{ion} for all simulations (Chimera, ASTER, xRAGE glue and xRAGE laser) are summarized in FIG. 16 for easy comparison of the results.

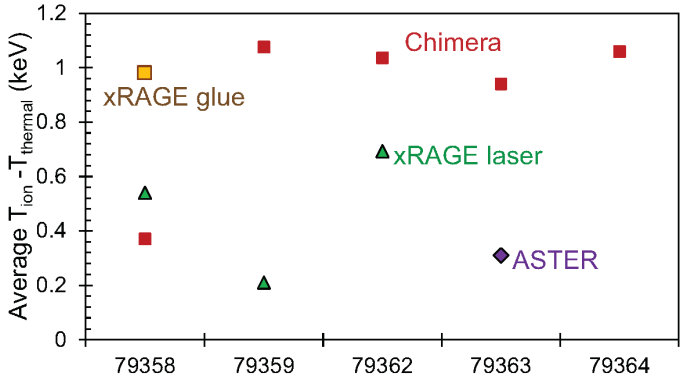


FIG. 16. Average simulated apparent T_{ion} minus thermal T_{ion} (i.e., expected flow enhancement) from all simulations studied for this paper.

Table VII summarizes the xRAGE-simulated yields. The yield degradation is surprisingly consistent between shots. The drive asymmetry has a 20 +/- 2% impact on the yield (according to these simulations, the imposed asymmetry for 79359 and 79362 does not do much more than the inherent drive asymmetry for 79358) and the glue spot has a 31 +/- 3% impact on the yield. Note that the majority of the difference in yield between the symmetric and asymmetric implosions is captured in 1D; this means xRAGE expects the yield reduction to be mostly due to the 10% lower average laser energy for the asymmetric implosions.

Table VII. xRAGE-simulated yields.

Shot	1D yield	2D as-shot drive	2D glue spot
79358	2.45E+13	2.01E+13	1.77E+13
79359	1.52E+13	1.23E+13	1.01E+13
79362	2.09E+13	1.64E+13	1.45E+13

IV. COMPARISON BETWEEN MEASURED AND SIMULATED RESULTS

In this section, measured and simulated T_{ion}, yield, x-ray images, burn history and ρR are compared, and implications of the comparisons discussed.

Ion temperature

Average measured apparent T_{ion} for each of our five implosions are contrasted to simulated in FIG. 17. Note that the average plotted is the average for all reporting detectors. This means the numbers are directly comparable for ASTER, Chimera and the measurements, which all report T_{ion} in the 12mntof, 15.8mntof and 5.0mcvd LOS. xRAGE on the other hand reports numbers parallel, antiparallel and perpendicular to the imposed asymmetry, which should be kept in mind when directly comparing numbers in FIG. 17. xRAGE and Chimera both appear to capture the overall level of T_{ion} relatively well. It is important to remember that while both the stalk mount and the drive asymmetry are expected to contribute to flow enhancement of T_{ion}, the two effects cannot be assumed to be directly additive. A 3D simulation including both effects would be a very interesting next step in this work. The Chimera-inferred average T_{ion} tracks the measurement remarkably well, with Chimera ~0.3 keV lower than measured on all implosions. While the reason for the systematic difference is not known, recall that the stalk mount not considered in the Chimera simulations is expected from xRAGE (Table VI) to contribute about 1 keV flow enhancement – this could easily make up the observed difference. The ASTER-inferred T_{ion} comes in significantly lower than measured for reasons that are not clear at this time. ASTER has been benchmarked against LILAC, and LILAC gets T_{ion} much closer to measured on these implosions (FIG. 9).

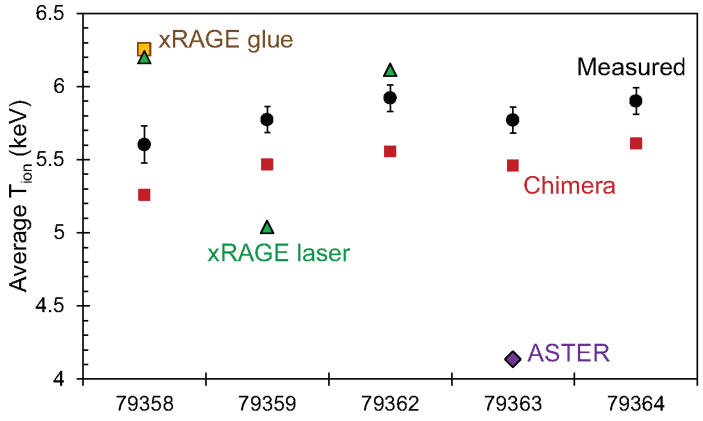


FIG. 17. Comparison of measured and simulated average T_{ion}.

As discussed in Ref. 26, Chimera quite closely reproduces the observed LOS asymmetry in T_{ion} for Asym. A, where an average T_{ion} enhancement of ~0.4 keV is seen parallel to the imposed mode 2 relative to the symmetric shot (compare Table V, FIG. 5), although the measured asymmetry is a little bit weaker than simulated. For Asym. B, more of an overall enhancement in T_{ion} relative to the symmetric shot is observed in the experiment, while Chimera still expects the enhancement parallel to the imposed mode 2 asymmetry. As discussed in Ref. 26, this comparison combined with the geometry of the experiment, with the stalk at

37° from Asym. A and 71° from Asym. B, suggests that the observations can be understood in terms of interplay of flows seeded by the imposed mode 2 and the stalk. As a reminder, the Chimera simulations do not consider the stalk mount. For Asym. A, the stalk at 37° to the mode 2 is conjectured to be enough to weaken the observed asymmetry, but not eliminate it. This interpretation is also supported by the fact that Chimera simulations with nominal compared to as-shot asymmetry showed how the as-shot asymmetry weakened the signature of the imposed asymmetry in the T_{ion} LOS variations, which is really another manifestation of interfering flows. For Asym. B, the stalk at 71° to the imposed mode 2 is conjectured to more directly counteract the imposed mode 2, with the interference between the two asymmetry seeds leading to eliminated LOS variations in T_{ion} but a significant remaining flow enhancement in average T_{ion}. We call this overall interpretation of the T_{ion} asymmetry results the "interplay hypothesis". This hypothesis is also further supported by x-ray self-emission imaging results and ρR asymmetry measurements, as discussed in Ref. 26 and further elaborated below. Obviously, a very interesting next step in fully confirming this hypothesis would again be 3D simulations including the imposed mode 2 and the stalk mount.

While the Chimera results can be reconciled with the data in this way, the xRAGE and ASTER results remain a question. The 2D geometry of the xRAGE simulations may dampen an observed asymmetry due to the artificial rotation of the problem. As discussed above, the sign of the observed asymmetry will depend very sensitively on the timing of outflow relative to peak burn; the dynamics of this process may also be impacted by the 2D vs 3D geometry. With these caveats, it is still interesting to note that the xRAGE simulations show the smallest expected LOS variations and the largest overall flow enhancement due to drive asymmetry for Asym. B implosion 79362 (Table VI) – this appears consistent with the experimental observation of very small LOS differences for Asym. B (FIG. 5).

The sensitive dependence of the T_{ion} asymmetry on the timing of outflow relative to burn (FIG. 12) makes the mode 2 impact on T_{ion} LOS signatures challenging to predict. For comparison, a mode 1 asymmetry is expected to very consistently show enhancement in inferred T_{ion} parallel to the asymmetry, with lowest T_{ion} observed perpendicular to the imposed mode 1 (FIG. 18). For this reason, a mode 1 might present a less challenging test of the capability of simulations to reproduce an imposed low-mode asymmetry. This will be tried in future experiments.

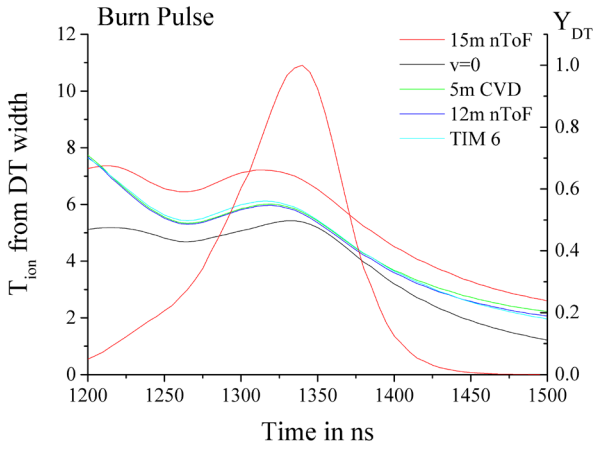


FIG. 18. Chimera-simulated T_{ion} versus time for a hypothetical implosion with a mode 1 induced by offsetting the target 30-μm towards the 15mntof detector. In this problem, the 15mntof detector (red) parallel to the imposed asymmetry gives maximum inferred T_{ion} throughout the duration of burn, while the 5.0mcvd (green), 12mntof (blue) and TIM6 (cyan; not used in the experiment) detectors all located approximately perpendicular to the imposed drive asymmetry give a lower inferred T_{ion}. The simulated burn pulse is shown in red (right scale). Because of the consistent sign of the asymmetry as a function of time, the impact of the mode 1 asymmetry on observed T_{ion} should be easier to predict than for mode 2 (compare FIG. 12).

Yield

Measured yields are listed in Table II, Chimera-simulated yields in Table V, and xRAGE-simulated yields in Table VII. Neither Chimera-simulated nor xRAGE-simulated absolute yields are expected to be directly comparable to the measured yields. Chimera does not consider ^{3}He in the fuel. Each of the xRAGE simulations (1D, 2D with glue, 2D with drive asymmetry) is missing some effect known to have an impact on yield. However, it is interesting to study the relative yields for the symmetric and asymmetric implosions (this comparison cannot be done for ASTER, which was not run for the symmetric shot). Measured and simulated yields relative to symmetric are shown in FIG. 19. The interpretation of these results is complicated by the significant variation in measured yield between the two Asym. A implosions (79359 and 79363) and the two Asym. B implosions (79362 and 79364). The simulations consider the small measured shot-to-shot differences in shell thickness, capsule size, fill pressure and as-shot laser energy for each implosion (Table I), so these factors cannot explain the observed yield variations. With the exception of xRAGE glue, the simulations do not consider the glue spots, but there is no obvious systematic difference between the glue spots used for shots 79359 and 79362 (lower yield) vs 79363 and 79364 (higher yield). With this caveat in mind, the first thing to note when looking at FIG. 19 is that the 1D xRAGE simulations capture a significant fraction of the observed yield reduction. Since the 1D simulations do not incorporate any asymmetries, this means that a large part of the yield reduction can be explained by the 10% reduced overall laser energy on the asymmetric shots. The second thing to note is that Chimera captures the yield reduction very well for shots 79359 and 79362, and actually overestimates the yield reduction for shots 79363 and 79364, leading to an average over-estimate of the yield reduction. We conjecture that the overestimate could be because Chimera does not include the stalk. Yield reduction due to the impact of the stalk mount is obviously expected to impact both symmetric and asymmetric implosions. The combined impact of stalk mount-induced yield reduction and laser asymmetry-induced yield reduction is unlikely to be directly additive, meaning the stalk mount alone could have a more significant impact on the symmetric implosion than the stalk mount on top of the imposed laser drive asymmetry on the asymmetric implosions.

The 2D xRAGE simulations all incorporate the laser energy reduction responsible for the yield reduction in the 1D xRAGE simulation. As can be seen from FIG. 19, both the laser drive asymmetry (2D xRAGE laser) and the glue spot (2D xRAGE glue) simulations lead to a slight expected additional yield reduction compared to the 1D simulations. Visually combining the impact of laser asymmetry and glue (and considering that the effects may not be directly additive), the xRAGE simulations appear to reproduce the average measured asymmetry extremely closely for the Asym. A shots (79359, 79363) and fairly closely for the Asym. B shots (79362, 79364).

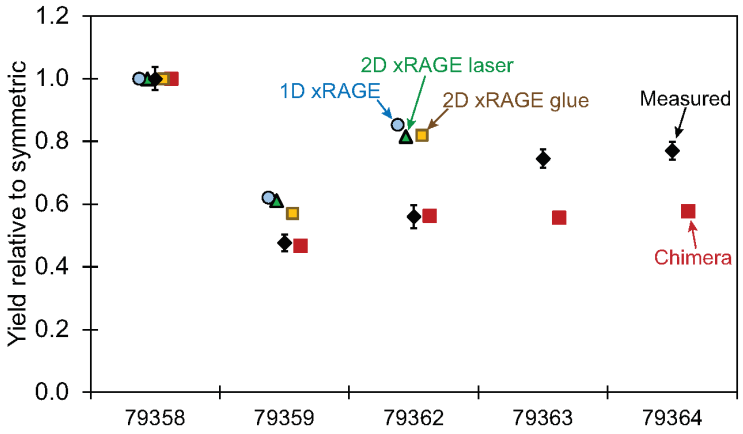


FIG. 19. Yield relative to symmetric as measured (black diamonds), simulated using Chimera (maroon squares), simulated using 1D xRAGE (blue circles), 2D RAGE with glue spot and no drive asymmetry (green triangles) and 2D RAGE with the imposed drive asymmetry but no glue spot (yellow squares).

Given the concerns about the impact of low-mode asymmetries on implosion performance,[2-4,6-11] the small apparent reduction resulting from the imposed mode 2 may be surprising. However, two factors should be kept in mind here. The first is that the detrimental impact of low mode asymmetries is expected to grow as a function of implosion convergence.[4,58] The implosions studied here are relatively low convergence, which explains why the effect is not so large. The second is that all of these implosions, including the symmetric reference, are subject to the detrimental impact of the stalk mount.

x-ray imaging: shell trajectory/mode 2

Implosion trajectories and mode 2 asymmetry amplitudes have been inferred from measured and synthetic self-emission x-ray images such as those shown in FIG. 8 using the method described in Ref. 49. The measured and simulated results are contrasted in FIG. 20. Synthetic x-ray images from Chimera are only available at late time, because of how the 3D simulation is initialized after the end of the laser pulse using HYADES simulations. FIG. 20a shows the comparison of measured and simulated implosion trajectories for Asym. A shot 79363, and FIG. 20b shows the same quantity for Asym. B implosion 79364. The xRAGE results shown come from the 2D drive asymmetry simulations (note that xRAGE results for shots 79359 and 79362 are used, since xRAGE was not run for 79363 and 79364). Excellent agreement is seen between measured and Chimera- and xRAGE simulated trajectories, which indicates that these simulations capture the overall hydrodynamics of the implosions extremely well. (The ASTER simulation of 79363 also captures the overall compression of the implosion well, but predicts a slightly slower implosion than observed in the data.)

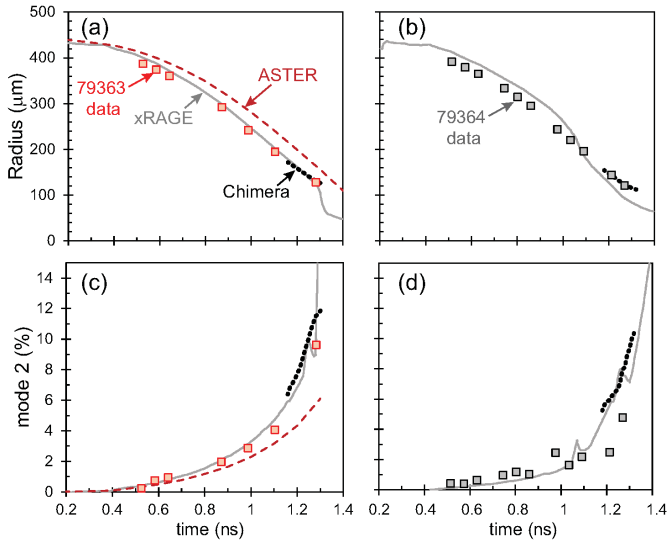


FIG. 20. Comparison of measured (square data points) and simulated (lines) shell trajectory (a,b) and mode 2 amplitude (c,d) inferred from self-emission x-ray imaging for Asym. A shot 79363 (a,c) and Asym. B shot 79364 (b,d). Solid gray lines represent xRAGE-simulated results (from the 2D drive asymmetry simulation), dashed red lines ASTER simulations, and dotted black Chimera simulations.

FIG. 20c,d show the mode 2 amplitude inferred from the self-emission x-ray images. (As mentioned above, the x-ray framing camera is expected to see 98% of the mode 2 for Asym. A and 67% of the mode 2 for Asym. B; this is considered in FIG. 20). We note that the mode 2 for Asym. A shot 79363 (panel c) is significantly better captured in both Chimera and xRAGE simulations than the mode 2 for Asym. B shot 79364. This is consistent with an effect not considered in the simulations (the stalk mount) interfering with the imposed mode 2 for Asym. B, supporting the interplay hypothesis outlined above and in Ref. 26.

Burn history

Bang times and burn histories for these experiments were measured using the OMEGA neutron temporal diagnostic (NTD).[59] Two separate and independent NTDs were used for the bang time measurement, one in OMEGA port H5 and one in port P11. The absolute uncertainty in each measurement is ±50ps. The H5 NTD was not well shielded and was unable to reliably measure burn-history on these implosions. Unfortunately, the P11 NTD failed on shot 79359, so no measured burn history is available for that implosion. The measured bang times are contrasted to xRAGE, ASTER and Chimera simulations in Table VIII. The xRAGE numbers quoted are from 1D simulations; there are some variations in 2D but they are small. Note that the xRAGE bang times are in excellent agreement with experiment. These simulations were performed using the laser ray trace to drive them and no adjustments were made to the drive. The Chimera-simulated bang times are also in excellent agreement with experiment. As described above, Chimera simulations were initialized with HYADES simulations mocking up the as-shot drive, with drive powers adjusted to match the measured laser absorption. The ASTER simulation bangs later than the experiment, consistent with the slower implosion trajectory seen in FIG. 20.

Table VIII. Measured and simulated bang times. Note that two NTD detectors, located in OMEGA diagnostic ports P11 and H5, were used to measure the bang time on these implosions, with the P11 results listed in normal print, the H5 results in italics.

Shot	Measured BT (ns) P11/*H5*	RAGE 1D BT (ns)	ASTER BT (ns)	CHIMERA BT (ns)
79358	1.36±0.05/*1.36±0.05*	1.35		1.359
79359	*1.41±0.05*	1.39		1.366
79362	1.36±0.05/*1.35±0.05*	1.39		1.362
79363	1.39±0.05/*1.37±0.05*		1.548	1.362
79364	1.36±0.05/*1.36±0.05*			1.357

To allow for direct comparison between measured and simulated burn histories, the simulated burn history must be broadened to account for the broadening effects impacting the measured data. These effects include[59]: the impulse response of the NTD (40±10 ps FWHM), thermal broadening of the DT neutron spectrum, and the finite neutron transit time through the scintillator (20 ps FWHM). Measured burn histories are contrasted to Chimera-simulated burn histories in FIG. 21. As can be seen, the burn width is captured remarkably well in the simulation. Considering the ±50ps uncertainty in the absolute timing of the NTD, the timing of burn is also well reproduced in the simulation.

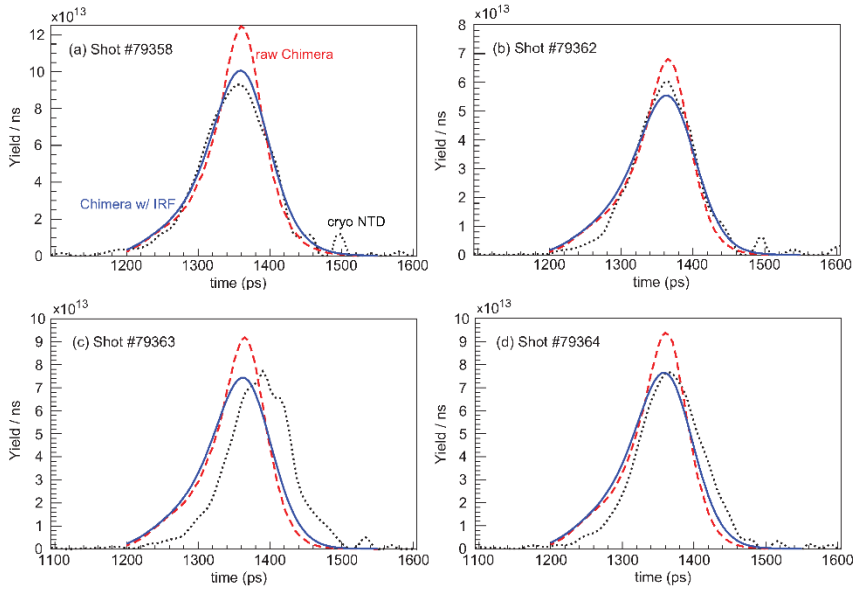


FIG. 21. Comparison of measured and Chimera-simulated burn histories for (a) shot 79358, (b) shot 79362, (c) shot 79363 and (d) shot 79364. All curves have been area normalized to the measured yield for easy comparison. The dotted black curve represents the measured burn history, the dashed red curve the raw Chimera-simulated burn history, and the solid blue the Chimera-simulated burn history considering broadening effects impacting the measurements. The solid blue and dashed black curves should be directly comparable.

The excellent agreement between Chimera simulations and measured burn histories (FIG. 21) as well as measured shell trajectories (FIG. 20) provides confidence in Chimera getting the hydrodynamics of the implosions right. However, it is important to note in this context that because of the very sensitive dependence on the T_{ion} asymmetry on the relative timing of outflow and burn (FIG. 12), any burn truncation

effects could have a significant impact on the predictions. It is conceivable that other perturbations apart from the imposed mode 2 and the stalk mount (e.g., higher mode perturbations) could cause the burn to truncate before there is significant outflows from the mode 2. If this happened, it could easily lead to the expected sign of the T_{ion} asymmetry flipping; since the nTOFs are only capturing the flow field during burn, they give no information on the flow field in the cold plasma after burn truncation.

Areal density

Implosion ρR has been inferred from the xRAGE, Chimera and LILAC simulations. Total ρR as a function of angle to the stalk determined from the xRAGE simulation with glue spot is contrasted to total ρR inferred from measured D^3He-p downshift in FIG. 22. Since this xRAGE simulation considers only the glue spot and not the imposed drive asymmetry, the most appropriate comparison is to the measured numbers for symmetric reference implosion 79358 (FIG. 22a). We find that while the xRAGE simulation underestimates the overall ρR amplitude, it closely reproduces the shape of the measured ρR. For the asymmetric implosions, we expect some additional impact from the imposed mode 2 not captured in the xRAGE simulations. The measurements for the asymmetric implosions consequently also show more scatter in inferred ρR (FIG. 22b,c). However, it is interesting to note that the xRAGE-predicted "weak spot" in ρR is seen in the measurements for all implosions. This provides clear evidence of the impact of the stalk on the implosions.

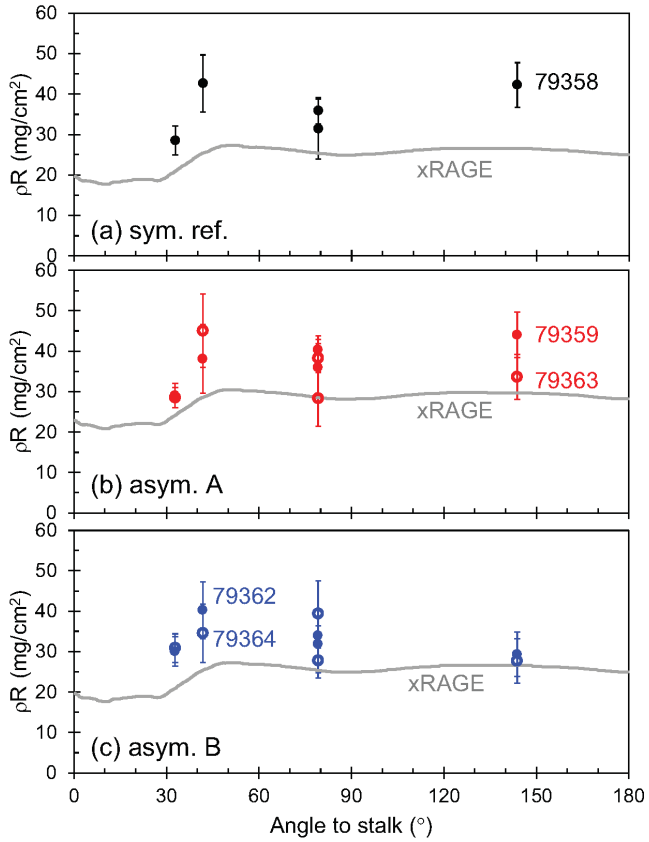


FIG. 22. Plot of total ρR measured on (a) symmetric reference implosion 79358, (b) Asym. A implosions 79359 and 79363, and (c) Asym. B implosions 79362 and 79364. Also shown in each panel is the xRAGE-simulated ρR (solid gray curve) for the glue spot only case.

The expected signature of mode 2 in the ρR distribution has been simulated using Chimera. Chimera-simulated, D^3He-burn-weighted total ρR for asymmetric implosions 79359 (Asym. A) and 79362 (Asym. B) are shown in FIG. 23a,b, together with the locations of the five proton spectrometers used in the experiment. As expected, the ρR asymmetry closely follows the imposed drive asymmetry, with weak spots in the region of low drive intensity, and higher ρR in the region of high drive intensity (compare FIG. 4). For easy comparison to the measurements in FIG. 22, the Chimera-simulated ρR in the LOS of each observing proton spectrometer is shown as a function of angle to the stalk and together with the 2D xRAGE-simulated ρR in FIG. 23c (although note that the scales are different between FIG. 22 and FIG. 23). We see that for Asym. A (red circles in FIG. 23c), the mode 2 drive asymmetry is expected to have a similar signature as the stalk. For Asym. B on the other hand, a relative enhancement in ρR is expected closest to the stalk due to the drive asymmetry. The fact that a weak spot is seen in the measured ρR in this region indicates that the impact of the stalk on the ρR dominates over the impact of the drive asymmetry. We also note that at the angles furthest from the stalk, the imposed drive asymmetry is expected to give rise to a relative weak spot in ρR for Asym. B and a relative enhancement for Asym. A; this difference is also observed in the measured data (compare FIG. 22 panels (b) and (c)).

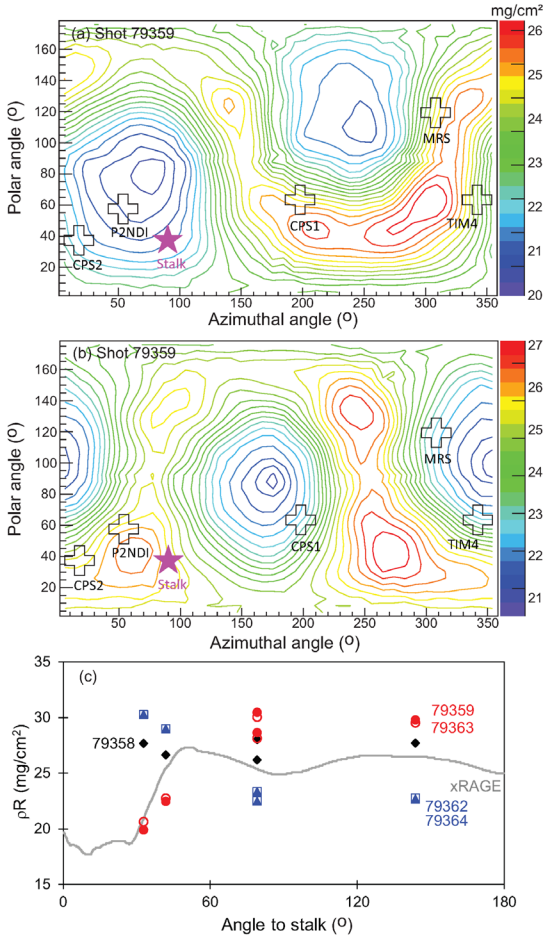


FIG. 23. Chimera-simulated total ρR, calculated from the center of the implosion and weighted by the D^3He burn history. Panels (a) and (b) show the angular ρR distributions for Asym. A shot 79359 and Asym. B shot 79362, respectively. Also indicated in these panels are the locations of the proton spectrometers used (plus signs) and of the stalk (star; note that the stalk is not considered in the Chimera simulations). Panel (c) shows the Chimera-simulated ρR in the LOS of the proton spectrometers used for each shot together with the 2D xRAGE-simulated ρR.

When comparing the absolute ρR values inferred from simulation and measurement, it is important to keep in mind that some assumptions are required to obtain a ρR from the measured D^3He-proton energy downshift. Recall that in the analysis for this paper, ρR's are inferred from the measured D^3He-p mean energy using 1D-simulated profiles of the implosion to correlate downshift to ρR (the 1D-profiles used for this are the LILAC-simulated t=1.5 ns profiles shown in FIG. 10). More work is needed to confirm that this gives accurate absolute numbers for asymmetric implosions. The most direct comparison would be between simulated and measured proton spectra. The capability to generate synthetic proton spectra from the Chimera simulations is under development, and will be used in future comparisons.

Burn-averaged total and shell ρR are also inferred from the 1D LILAC simulation. These numbers are contrasted to measurements for shot 79363 in FIG. 24. As can be seen, in contrast to xRAGE and Chimera, LILAC more closely reproduces the measured level of both shell and total ρR.

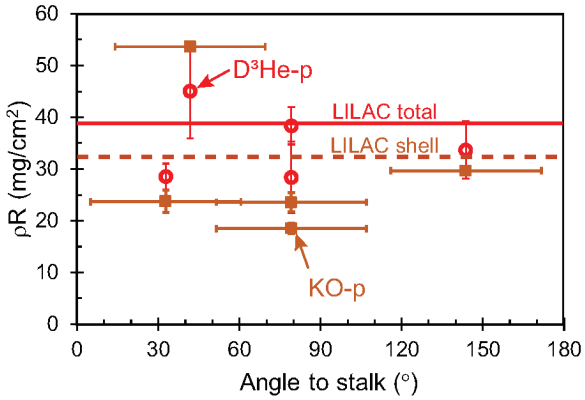


FIG. 24. Comparison between 1D-LILAC-simulated (lines) and measured (points with error bars) ρR, with total ρR (D^3He-p) shown as a red solid line and hollow circles, and shell ρR (KO-p) as a brown dashed line and solid squares.

V. SUMMARY AND CONCLUSIONS

In this paper, we have described a set of experiments with a mode 2 asymmetry in the laser drive intentionally imposed to test our ability to predict and measure the impact of this asymmetry on fuel flows in the implosion, and their impact on LOS variations in T_{ion}. The overarching goals of this experiment were to learn to interpret signatures in neutron spectra in terms of the velocity field in the implosion, and more broadly to develop an understanding for the velocity field in the implosion and how closely measured T_{ion} represents thermal T_{ion}.

We importantly conclude from this work that interference between flows introduced from different asymmetry seeds must be considered when interpreting the results (the interplay hypothesis; this conclusion was first reported in Ref. 26). Specifically, the results are expected to be well captured by a combination of flow seeded by the induced mode 2 asymmetry and flow seeded by the capsule stalk mount. This conclusion is based on comparison of 3D Chimera simulations not including the stalk with measured T_{ion} LOS asymmetry data and with measured self-emission x-ray imaging of the mode 2 amplitude.

The impact of the stalk is also evidenced by the experimental confirmation of a ρR "weak spot" in the vicinity of the stalk predicted from 2D xRAGE simulations including the stalk mount. This result clearly indicates the importance of the stalk as an asymmetry seed impacting OMEGA direct drive implosions. Interestingly, recent statistical analysis of results from OMEGA cryogenically layered implosions

compared with simulations indicates the presence of a systematic asymmetry seed for all implosions;[5] the present work suggests that this asymmetry seed is most likely the stalk.

We note that non-Maxwellian ion distributions due to tail ion depletion[60,61] would not impact the conclusions in this paper. The effect of such distribution modifications would be to reduce the observed thermal T_{ion}, because the lost highest-energy ions will no longer be available to undergo fusion and thus to generate neutrons. This paper addresses line-of-sight-dependent enhancement over thermal in the measured T_{ion} due to asymmetric flows. Such flow enhancement will not be impacted by non-Maxwellian effects.

As discussed in Ref. 26, the interplay hypothesis allows for self-consistent interpretation of observations from cryogenically layered implosions at OMEGA and the National Ignition Facility (NIF) previously found hard to reconcile. On NIF implosions, large differences in inferred DD and DT T_{ion} indicate the presence of flow, while minimal LOS variations in T_{ion} are observed.[17] On OMEGA, on the other hand, large LOS variations in T_{ion} have been routinely observed.[4,57] On the NIF, implosions are expected to be impacted by a mode 2 in the laser,[62,63] a mode 4 from the capsule support mount ("tent"),[64,65,66] and a mode 1 from the fill tube.[64] With the interplay hypothesis in mind, it is easy to imagine how interference of flows from these various sources could give rise to large flows but small observable T_{ion} asymmetries. OMEGA implosions, on the other hand, are expected to be impacted by a mode 1 asymmetry in the laser drive,[11] mode 1 due to the stalk[35,36] and mode 1 due to capsule offsets.[9] When the various asymmetry seeds align, we would expect large T_{ion} variations, while when they do not, smaller variations would be expected.

All simulations brought to bear to model the asymmetries discussed in this paper, including 3D ASTER, 3D Chimera and 2D xRAGE, indicate that thermal T_{ion} in these implosions is substantially lower than T_{ion} inferred from neutron spectra. Simulations including 1D LILAC also show a $T_{electron}$ that is significantly different than T_{ion}, emphasizing the importance of considering expected differences when attempting to measure $T_{electron}$ to get at the thermal T_{ion}.

To fully nail down the impact of low-mode asymmetries on implosion flow field and performance, and to learn how to mitigate these effects, improved simulations will be required. All simulation tools used in this work are seen to have some capability to capture the effect of asymmetry seeds, but all are missing some important aspect of the problem with no single simulation capturing all effects at play. Significant differences are also observed in the results obtained from the different simulation tools. Future work should include full 3D simulations considering the capsule stalk mount, as well as further benchmarking experiments with known seeded asymmetries.

ACKNOWLEDGEMENTS

The authors sincerely thank the OMEGA operations staff who supported this work, Bob Frankel and Ernie Doeg for processing the CR-39, and Michelle Evans for characterizing the target glue spots. This material is based upon work supported by the Department of Energy, National Nuclear Security Administration under Award Number DE-NA0002949, by the National Laser Users' Facility under award number DE-NA0002726, by LLE under award number 415935-G, and by Los Alamos National Laboratory operated by Los Alamos National Security, LLC for the U.S. Department of Energy NNSA under Contract No. DE-AC52-06NA25396. This report was prepared as an account of work sponsored by an agency of the United States Government. Neither the United States Government nor any agency thereof, nor any of their employees, makes any warranty, express or implied, or assumes any legal liability or responsibility for the accuracy, completeness, or usefulness of any information, apparatus, product, or process disclosed, or represents that its use would not infringe privately owned rights. Reference herein to any specific

commercial product, process, or service by trade name, trademark, manufacturer, or otherwise does not necessarily constitute or imply its endorsement, recommendation, or favoring by the United States Government or any agency thereof. The views and opinions of authors expressed herein do not necessarily state or reflect those of the United States Government or any agency thereof.

REFERENCES

[1] S. Atzeni & J. Meyer-Ter-Vehn, The Physics of Inertial Fusion, Oxford University Press (2004).

[2] O.A. Hurricane, D.A. Callahan, D.T. Casey, E.L. Dewald, T.R. Dittrich, T. Döppner, S. Haan, D.E. Hinkel, L.F. Berzak Hopkins, O. Jones, A.L. Kritcher, S. Le Pape, T. Ma, A.G. MacPhee, J.L. Milovich, J. Moody, A. Pak, H.-S. Park, P.K. Patel, J.E. Ralph, H.F. Robey, J.S. Ross, J.D. Salmonson, B.K. Spears, P.T. Springer, R. Tommasini, F. Albert, L.R. Benedetti, R. Bionta, E Bond, D.K. Bradley, J. Caggiano, P.M. Celliers, C. Cerjan, J.A. Church, R. Dylla-Spears, D. Edgell, M.J. Edwards, D. Fittinghoff, M.A. Barrios Garcia, A. Hamza, R. Hatarik, H. Herrmann, M. Hohenberger, D. Hoover, J.L. Kline, G. Kyrala, B. Kozioziemski, G. Grim, J.E. Field, J. Frenje, N. Izumi, M. Gatu Johnson, S.F. Khan, J. Knauer, T. Kohut, O. Landen, F. Merrill, P. Michel, S.R. Nagel, A. Nikroo, T. Parham, R.R. Rygg, D. Sayre, M. Schneider, D. Shaughnessy, D. Strozzi, R.P.J. Town, D. Turnbull, P. Volegov, A. Wan, K. Widmann, C. Wilde and C. Yeamans, Nature Physics **12**, 800 (2016). (DOI: 10.1038/NPHYS3720)

[3] S. LePape, L. F. Berzak Hopkins, L. Divol, A. Pak, E. L. Dewald, S. Bhandarkar, L. R. Bennedetti, T. Bunn, J. Biener, J. Crippen, D. Casey, D. Edgell, D. N. Fittinghoff, M. Gatu-Johnson, C. Goyon, S. Haan, R. Hatarik, M. Havre, D. D-M. Ho, N. Izumi, J. Jaquez, S. F. Khan, G. A. Kyrala, T. Ma, A. J. Mackinnon, A. G. MacPhee, B. J. MacGowan, N. B. Meezan, J. Milovich, M. Millot, P. Michel, S. R. Nagel, A. Nikroo, P. Patel, J. Ralph, J. S. Ross, N. G. Rice, D. Strozzi, M. Stadermann, P. Volegov, C. Yeamans, C. Weber, C. Wild, D. Callahan, and O. A. Hurricane, Phys. Rev. Lett. **120**, 245003 (2018).

[4] S.P. Regan, V. N. Goncharov, I. V. Igumenshchev, T. C. Sangster, R. Betti, A. Bose, T. R. Boehly, M. J. Bonino, E. M. Campbell, D. Cao, T. J. B. Collins, R. S. Craxton, A. K. Davis, J. A. Delettrez, D. H. Edgell, R. Epstein, C. J. Forrest, J. A. Frenje, D. H. Froula, M. Gatu Johnson, V. Yu. Glebov, D. R. Harding, M. Hohenberger, S. X. Hu, D. Jacobs-Perkins, R. Janezic, M. Karasik, R. L. Keck, J. H. Kelly, T. J. Kessler, J. P. Knauer, T. Z. Kosc, S. J. Loucks, J. A. Marozas, F. J. Marshall, R. L. McCrory, P.W. McKenty, D. D. Meyerhofer, D. T. Michel, J. F. Myatt, S. P. Obenschain, R. D. Petrasso, P. B. Radha, B. Rice, M. J. Rosenberg, A. J. Schmitt, M. J. Schmitt, W. Seka, W. T. Shmayda, M. J. Shoup III, A. Shvydky, S. Skupsky, A. A. Solodov, C. Stoeckl, W. Theobald, J. Ulreich, M. D. Wittman, K. M. Woo, B. Yaakobi, and J. D. Zuegel, Phys. Rev. Lett. **117**, 025001 (2016).

[5] V. Gopalaswamy, R. Betti, J.P. Knauer, I.V. Igumenshchev, A. Bose, N. Luciani, K.M. Woo, D. Patel, A.R. Christopherson, O.M. Mannion, S. Miller, F.J. Marshall, C. Stoeckl, V.Yu. Glebov, S.P. Regan, D.T. Michel, W. Seka, R.C. Shah, D.H. Edgell, D.W. Jacobs-Perkins, D. Cao, S.F.B. Morse, R.T. Janezic, J.H. Kelly, S. Sampat, K. Bauer, V.N. Goncharov, J.A. Delettrez, J.R. Davies, A.B. Sefkow, R. Epstein, P.B. Radha, T.J.B. Collins, S.X. Hu, C.J. Forrest, T.C. Sangster, G.W. Collins, E.M. Campbell, M. Gatu Johnson, R.D. Petrasso, C.K. Li and J.A. Frenje, "Tripling the Fusion Yield in Direct-Drive Laser Fusion through Data-Driven Statistical Modeling", submitted to Nature (2018).

[6] B.K. Spears, M.J. Edwards, S. Hatchett, J. Kilkenny, J. Knauer, A. Kritcher, J. Lindl, D. Munro, P. Patel, H.F. Robey, and R.P.J. Town, Phys. Plasmas **21**, 042702 (2014).

[7] A. L. Kritcher, R. Town, D. Bradley, D. Clark, B. Spears, O. Jones, S. Haan, P. T. Springer, J. Lindl, R. H. H. Scott, D. Callahan, M. J. Edwards, and O. L. Landen, Phys. Plasmas **21**, 042708 (2014).

[8] A. L. Kritcher, D. E. Hinkel, D. A. Callahan, O. A. Hurricane, D. Clark, D. T. Casey, E. L. Dewald, T. R. Dittrich, T. Döppner, M. A. Barrios Garcia, S. Haan, L. F. Berzak Hopkins, O. Jones, O. Landen, T. Ma, N. Meezan, J. L. Milovich, A. E. Pak, H.-S. Park, P. K. Patel, J. Ralph, H. F. Robey, J. D. Salmonson, S. Sepke, B. Spears, P. T. Springer, C. A. Thomas, R. Town, P. M. Celliers, and M. J. Edwards, Phys. Plasmas **23**, 052709 (2016).

[9] I.V. Igumenshchev, V.N. Goncharov, F.J. Marshall, J.P. Knauer, E.M. Campbell, C.J. Forrest, D.H. Froula, V.Yu. Glebov, R.L. McCrory, S.P. Regan, T.C. Sangster, S. Skupsky and C. Stoeckl, Phys. Plasmas **23**, 052702 (2016).

[10] I.V. Igumenshchev, D.T. Michel, R.C. Shah, E.M. Campbell, R. Epstein, C.J. Forrest, V.Yu. Glebov, V.N. Goncharov, J.P. Knauer, F.J. Marshall, R.L. McCrory, S.P. Regan, T.C. Sangster, C. Stoeckl, A.J. Schmitt and S. Obenschein, Phys. Plasmas **24**, 056307 (2017).

[11] R.C. Shah, B.M. Haines, F.J. Wysocki, J.F. Benage, J.A. Fooks, V. Glebov, P. Hakel, M. Hoppe, I.V. Igumenshchev, G. Kagan, R.C. Mancini, F.J. Marshall, D.T. Michel, T.J. Murphy, M.E. Schoff, K. Silverstein, C. Stoeckl and B. Yaakobi, Phys. Rev. Lett. **118**, 135001 (2017).

[12] P. T. Springer, O. A. Hurricane, J. H. Hammer, R. Betti, D. A. Callahan, E. M. Campbell, D. T. Casey, C. J. Cerjan, D. Cao, E. Dewald, L. Divol, T. Doeppner, M. J. Edwards, J. E. Field, C. Forrest, J. Frenje, J. A. Gaffney, M. Gatu-

Johnson, V. Glebov, V. N. Goncharov, G. P. Grim, E. Hartouni, R. Hatarik, D. E. Hinkel, L. F. B. Hopkins, I. Igumenshchev, P Knapp, J. P. Knauer, A.L. Kritcher, O. Landen, A. Pak, S. Le Pape, T. Ma, A. G. MacPhee, D. H. Munro, R. C. Nora, P. K. Patel, L. Peterson, P. B. Radha, S. P. Regan, H. Rinderknecht, C. Sangster, B. K. Spears, C. Stoeckl, A 3D dynamic model to assess impacts of low-mode asymmetry, aneurysms, and mix induced radiative loss on capsule performance across ICF platforms, submitted to Nuclear Fusion (2018).
[13] L. Ballabio, J. Källne, and G. Gorini, Nucl. Fusion **38**, 1723 (1998).
[14] $\Delta E_n \approx 0.177 \times \sqrt{T_{ion}}$, with ΔE_n the FWHM of the primary DT neutron peak in MeV, and T_{ion} in keV.
[15] B. Appelbe and J. Chittenden, Plasma Phys. Control. Fusion 53, 045002 (2011).
[16] T. J. Murphy, Phys. Plasmas 21, 072701 (2014).
[17] M. Gatu Johnson, J.P. Knauer, C.J. Cerjan, M.J. Eckart, G.P. Grim, E.P. Hartouni, R. Hatarik, J.D. Kilkenny, D.H. Munro, D.B. Sayre, B.K. Spears, R.M. Bionta, E.J. Bond, J.A. Caggiano, D. Callahan, D.T. Casey, T. Döppner, J.A. Frenje, V.Yu. Glebov, O. Hurricane, A. Kritcher, S. LePape, T. Ma, A. Mackinnon, N. Meezan, P. Patel, R.D. Petrasso, J.E. Ralph, P.T. Springer, and C.B. Yeamans, Phys. Rev. E **94**, 021202(R) (2016).
[18] J. L. Peterson, K.D. Humbird, J.E. Field, S.T. Brandon, S.H. Langer, R.C. Nora, B.K. Spears and P.T. Springer, Phys. Plasmas **24**, 032702 (2017).
[19] R. Betti, P.Y. Chang, B. K. Spears, K.S. Anderson, J. Edwards, M. Fatenejad, J.D. Lindl, R.L. McCrory, R. Nora and D. Shvarts, Phys. Plasmas 17, 058102 (2010).
[20] R. Betti, A.R. Christopherson, B.K. Spears, R. Nora, A. Bose, J. Howard, K.M. Woo, M.J. Edwards and J. Sanz, Phys. Rev. Lett. 114, 255003 (2015).
[21] T.R. Boehly, D.L. Brown, R.S. Craxton, R.L. Keck, J.P. Knauer, J.H. Kelly, T.J. Kessler, S.A. Kumpan, S.J. Loucks, S.A. Letzring, F.J. Marshall, R.L. McCrory, S.F.B. Morse, W. Seka, J.M. Soures, and C.P. Verdon, Opt. Commun. 133, 495 (1997).
[22] C.R. Christensen, D.C. Wilson, C.W. Barnes, G.P. Grim, G.L. Morgan, M.D. Wilke, F.J. Marshall, V.Yu. Glebov and C. Stoeckl, Phys. Plasmas **11**, 2771 (2004).
[23] J.A. Cobble, T.J. Murphy, M.J. Schmitt, P.A. Bradley, N.S. Krashenninikova, K.A. Obrey, S.C. Hsu, I.L. Tregillis, G.R. Magelssen, F.J. Wysocki, and S.H. Batha, Phys. Plasmas **19**, 122713 (2012).
[24] C. R. Danly, T. H. Day, D. N. Fittinghoff, H. Herrmann, N. Izumi, Y. H. Kim, J. I. Martinez, F. E. Merrill, D. W. Schmidt, R. A. Simpson, P. L. Volegov, and C. H. Wilde, Rev. Sci. Instrum. **86**, 043503 (2015).
[25] F.H. Séguin, C.K. Li, J.L. DeCiantis, J.A. Frenje, J.R. Rygg, R.D. Petrasso, F.J. Marshall, V. Smalyuk, V.Yu. Glebov, J.P. Knauer, T.C. Sangster, J.D. Kilkenny and A. Nikroo, Phys. Plasmas **23**, 032705 (2016).
[26] M. Gatu Johnson, B.D. Appelbe, J.P. Chittenden, J. Delettrez, C. Forrest, J.A. Frenje, V.Yu. Glebov, W. Grimble, B.M. Haines, I. Igumenshchev, R. Janezic, J.P. Knauer, B. Lahmann, F. Marshall, T. Michel, F.H. Séguin, C. Stoeckl, C. Walsh, A.B. Zylstra, R.D. Petrasso, "Impact of asymmetries on fuel performance in Inertial Confinement Fusion", Phys. Rev. E **98**, 051201(R) (2018).
[27] V.Yu. Glebov, T. C. Sangster, C. Stoeckl, J. P. Knauer, W. Theobald, K. L. Marshall, M. J. Shoup III, T. Buczek, M. Cruz, T. Duffy, M. Romanofsky, M. Fox, A. Pruyne, M. J. Moran, R. A. Lerche, J. McNaney, J. D. Kilkenny, M. J. Eckart, D. Schneider, D. Munro, W. Stoeffl, R. Zacharias, J. J. Haslam, T. Clancy, M. Yeoman, D. Warwas, C. J. Horsfield, J.-L. Bourgade, O. Landoas, L. Disdier, G. A. Chandler, and R. J. Leeper, Rev. Sci. Instrum. **81**, 10D325 (2010).
[28] University of Rochester, Laboratory for Laser Energetics, National Laser Users' Facility Users Guide, http://www.lle.rochester.edu/media/about/documents/UsersGuide/05_UsersGuide.pdf (2014).
[29] V.Yu. Glebov, "Six DT nTOF detectors on OMEGA", nTOF Diagnostic Workshop, LLNL, July 18 (2017).
[30] J. J. MacFarlane, J. Quant. Spectrosc. Radiat. Transf. 81, 287 (2003).
[31] S. Skupsky, R.W. Short, T. Kessler, R.S. Craxton, S. Letzring, and J.M. Soures, J. Appl. Phys. 66, 3456 (1989); S.P. Regan, John A. Marozas, R. Stephen Craxton, John H. Kelly, William R. Donaldson, Paul A. Jaanimagi, Douglas Jacobs-Perkins, Robert L. Keck, Terrance J. Kessler, David D. Meyerhofer, T. Craig Sangster, Wolf Seka, Vladimir A. Smalyuk, Stanley Skupsky, and Jonathan D. Zuegel, J. Opt. Soc. Am. B 22, 998 (2005).
[32] T.R. Boehly, V.A. Smalyuk, D.D. Meyerhofer, J.P. Knauer, D.K. Bradley, R.S. Craxton, M.J. Guardalben, S. Skupsky and T.J. Kessler, J. Appl. Phys. 85, 3444 (1999).
[33] F.J. Marshall, J.A. Delettrez, R. Epstein, R. Forties, R.L. Keck, J.H. Kelly, P.W. McKenty, S.P. Regan and L.J. Waxer, Phys. Plasmas 11, 251 (2004).
[34] J.R. Rygg, J.A. Frenje, C.K. Li, F.H. Séguin, R.D. Petrasso, F.J. Marshall, J.A. Delettrez, J.P. Knauer, D.D. Meyerhofer, and C. Stoeckl, Phys. Plasmas 15, 034505 (2008).
[35] I.V. Igumenshchev, F.J. Marshall, J.A. Marozas, V.A. Smalyuk, R. Epstein, V.N. Goncharov, T.J.B. Collins, T.C. Sangster, and S. Skupsky, Phys. Plasmas 16, 082701 (2009).
[36] Brian M. Haines, Gary P. Grim, James R. Fincke, Rahul C. Shah, Chad J. Forrest, Kevin Silverstein, Frederic J. Marshall, Melissa Boswell, Malcolm M. Fowler, Robert A. Gore, Anna C. Hayes-Sterbenz, Gerard Jungman, Andreas Klein, Robert S. Rundberg, Michael J. Steinkamp, and Jerry B. Wilhelmy, Phys. Plasmas **23**, 072709 (2016).

[37] C. Stoeckl, R. Epstein, R. Betti, W. Bittle, J. A. Delettrez, C. J. Forrest, V. Yu. Glebov, V. N. Goncharov, D. R. Harding, I. V. Igumenshchev, D. W. Jacobs-Perkins, R. T. Janezic, J. H. Kelly, T. Z. Kosc, R. L. McCrory, D.T. Michel, C. Mileham, P. W. McKenty, F. J. Marshall, S. F. B. Morse, S. P. Regan, P. B. Radha, B. Rice, T. C. Sangster, M. J. ShoupIII, W. T. Shmayda, C. Sorce, W. Theobald, J. Ulreich, M. D. Wittman, D. D. Meyerhofer, J. A. Frenje, M. Gatu Johnson, and R. D. Petrasso, Phys. Plasmas **24**, 056304 (2017).
[38] University of Rochester, Laboratory for Laser Energetics, National Laser Users' Facility Users Guide, http://www.lle.rochester.edu/media/omega_facility/documentation/documents/nluf_users_guide.pdf (2007).
[39] W.R. Donaldson, J. Katz, R. Huff, E.M. Hill, J.H. Kelly, J. Kwiatkowski, R.B. Brannon, and R. Boni, Rev. Sci. Instrum. 87, 053511 (2016).
[40] W. Grimble, F.J. Marshall, and E. Lambrides, Phys. Plasmas **25**, 072702 (2018); LLE Review, Vol. 151, p.146-151 (2017).
[41] F. H. Séguin, J. A. Frenje, C. K. Li, D. G. Hicks, S. Kurebayashi, J. R. Rygg, B.-E. Schwartz, R. D. Petrasso, S. Roberts, J. M. Soures, D. D. Meyerhofer, T. C. Sangster, J. P. Knauer, C. Sorce, V. Yu. Glebov, C. Stoeckl, T. W. Phillips, R. J. Leeper, K. Fletcher and S. Padalino, Rev. Sci. Instrum. 74, 975 (2003).
[42] D. T. Casey,J. A. Frenje, M. Gatu Johnson, F. H. Séguin, C. K. Li, R. D. Petrasso, V. Yu. Glebov, J. Katz, J. Magoon, D. D. Meyerhofer, T. C. Sangster, M. Shoup, J. Ulreich, R. C. Ashabranner, R. M. Bionta, A. C. Carpenter, B. Felker, H. Y. Khater, S. LePape, A. MacKinnon, M. A. Mckernan, M. Moran, J. R. Rygg, M. F. Yeoman, R. Zacharias, R. J. Leeper, K. Fletcher, M. Farrell, D. Jasion, J. Kilkenny, and R. Paguio, Rev. Sci. Inst. **84**, 043506 (2013).
[43] D. Hicks, "Charged-Particle Spectroscopy: A new window on Inertial Confinement Fusion", PhD Thesis, Massachusetts Institute of Technology (1999).
[44] J. R. Rygg, J. A. Frenje, C. K. Li, F. H. Séguin, R. D. Petrasso, J. A. Delettrez, V. Y. Glebov, V. N. Goncharov, D. D. Meyerhofer, S. P. Regan, T. C. Sangster, and C. Stoeckl, Phys. Plasmas **13**, 052702 (2006).
[45] H.-S. Bosch and G.M. Hale, Nucl. Fusion **32**, 611 (1992).
[46] MCNPX User's Manual, Version 2.7.0, LA-CP-11-00438, April 2011, see https://mcnpx.lanl.gov.
[47] F.H. Séguin, C.K. Li, J.A. Frenje, S. Kurebayashi, R.D. Petrasso, F.J. Marshall, D.D. Meyerhofer, J.M. Soures, T.C. Sangster, C. Stoeckl, J.A. Delettrez, P.B. Radha, V.A. Smalyuk, and S. Roberts, Phys. Plasmas **9**, 3558 (2002).
[48] C.K. Li, F.H. Séguin, D.G. Hicks, J.A. Frenje, K.M. Green, S. Kurebayashi, R.D. Petrasso, D.D. Meyerhofer, J.M. Soures, V.Yu. Glebov, R.L. Keck, P.B. Radha, S. Roberts, W. Seka, S. Skupsky and C. Stoeckl, Phys. Plasmas **8**, 4902 (2001).
[49] D.T. Michel, A.K. Davis, W. Armstrong, R. Bahr, R. Epstein, V.N. Goncharov, M. Hohenberger, I.V. Igumenshchev, R. Jungquist, D.D. Meyerhofer, P.B. Radha, T.C. Sangster, C. Sorce and D.H. Froula, High Power Laser Science and Engineering 3, e19 (2015). doi:10.1017/hpl.2015.15
[50] W. Seka, H.A. Baldis, J. Fuchs, S.P. Regan, D.D. Meyerhofer, C. Stoeckl, B. Yaakobi, R.S. Craxton and R.W. Short, Phys. Rev. Lett. 89, 175002 (2002).
[51] J. Delettrez, R. Epstein, M.C. Richardson, P.A. Jaanimagi, and B.L. Henke, Phys. Rev. A **36**, 3926 (1987).
[52] M. Gittings, R. Weaver, M. Clover, T. Betlach, N. Byrne, R. Coker, E. Dendy, R. Hueckstaedt, K. New, W.R. Oakes, D. Ranta and R. Stefan, Comput. Sci. Discovery 1, 015005 (2008).
[53] B.M. Haines, C.H. Aldrich, J.M. Campbell, R.M. Rauenzahn and C.A. Wingate, Phys. Plasmas 24, 052701 (2017).
[54] J.P. Chittenden, B.D. Appelbe, F. Manke, K. McGlinchey, and N.P.L. Niasse, Phys. Plasmas 23, 052708 (2016).
[55] J.T. Larsen and S.M. Lane, J. Quant. Spectrosc. Radiat. Transfer 51, 179 (1994).
[56] O.A. Hurricane, D. A. Callahan, D. T. Casey, P. M. Celliers, C. Cerjan, E. L. Dewald, T. R. Dittrich, T. Döppner, D. E. Hinkel, L. F. Berzak Hopkins, J. L. Kline, S. Le Pape, T. Ma, A. G. MacPhee, J. L. Milovich, A. Pak, H.-S. Park, P. K. Patel, B. A. Remington, J. D. Salmonson, P. T. Springer & R. Tommasini, Nature **506**, 343 (2014).
[57] Goncharov, Valeri; Regan, Sean; Campbell, Michael ; Sangster, Thomas; Radha, P; Myatt, Jason; Froula, Dustin; Betti, Riccardo; Boehly, Tom; Delettrez, J; Edgell, Dana; Epstein, Reuben; Forrest, Chad; Glebov, V; Harding, David; Hu, Suxing; Igumenshchev, Igor; Marshall, Frederic; McCrory, Robert; Michel, David; Seka, Wolf; Shvydky, A; Stoeckl, Christian; Theobald, Wolfgang; Gatu Johnson, Maria, Plasma Physics and Controlled Fusion **59**, 014008 (2017).
[58] B. M. Haines, S. A. Yi, R. E. Olson, S. F. Khan, G. A. Kyrala, A. B. Zylstra, P. A. Bradley, R. R. Peterson, J. L. Kline, R. J. Leeper, and R. C. Shah, Phys. Plasmas **24**, 072709 (2017).
[59] C. Stoeckl, R. Boni, F. Ehrne, C.J. Forrest, V. Yu. Glebov, J. Katz, D.J. Lonobile, J. Magoon, S.P. Regan, M.J. Shoup III, A. Sorce, C. Sorce, T.C. Sangster and D. Weiner, Rev. Sci. Instrum. **87**, 053501 (2016).
[60] K. Molvig, N.M. Hoffman, B.J. Albright, E.M. Nelson, and R.B. Webster, Phys. Rev. Lett. **109**, 095001 (2012).
[61] B.J. Albright, K. Molvig, C.-K. Huang, A.N. Simakov, E.S. Dodd, N.M. Hoffman, G. Kagan, and P.F. Schmit, Phys. Plasmas **20**, 122705 (2013).
[62] L. Divol, A. Pak, L. F. Berzak Hopkins, S. Le Pape, N. B. Meezan, E. L. Dewald, D. D.-M. Ho, S. F. Khan, A. J. Mackinnon, J. S. Ross, D. P. Turnbull, C. Weber, P. M. Celliers, M. Millot, L. R. Benedetti, J. E. Field, N. Izumi, G.

A. Kyrala, T. Ma, S. R. Nagel, J. R. Rygg, D. Edgell, A. G. Macphee, C. Goyon, M. Hohenberger, B. J. MacGowan, P. Michel, D. Strozzi, W. Cassata, D. Casey, D. N. Fittinghoff, N. Gharibyan, R. Hatarik, D. Sayre, P. Volegov, C. Yeamans, B. Bachmann, T. Döppner, J. Biener, J. Crippen, C. Choate, H. Huang, C. Kong, A. Nikroo, N. G. Rice, M. Stadermann, S. D. Bhandarkar, S. Haan, B. Kozioziemski, W. W. Hsing, O. L. Landen, J. D. Moody, R. P. J. Town, D. A. Callahan, O. A. Hurricane, and M. J. Edwards, Phys. Plasmas **24**, 056309 (2017).

[63] A. Pak, L. Divol, A. L. Kritcher, T. Ma, J. E. Ralph, B. Bachmann, L. R. Benedetti, D. T. Casey, P. M. Celliers, E. L. Dewald, T. Döppner, J. E. Field, D. E. Fratanduono, L. F. Berzak Hopkins, N. Izumi, S. F. Khan, O. L. Landen, G. A. Kyrala, S. LePape, M. Millot, J. L. Milovich, A. S. Moore, S. R. Nagel, H.-S. Park, J. R. Rygg, D. K. Bradley, D. A. Callahan, D. E. Hinkel, W. W. Hsing, O. A. Hurricane, N. B. Meezan, J. D. Moody, P. Patel, H. F. Robey, M. B. Schneider, R. P. J. Town, and M. J. Edwards, Phys. Plasmas **24**, 056306 (2017).

[64] C.R. Weber, D. T. Casey, D. S. Clark, B. A. Hammel, A. MacPhee, J. Milovich, D. Martinez, H. F. Robey, V. A. Smalyuk, M. Stadermann, P. Amendt, S. Bhandarkar, B. Chang, C. Choate, J. Crippen, S. J. Felker, J. E. Field, S. W. Haan, S. Johnson, J. J. Kroll, O. L. Landen, M. Marinak, M. Mcinnis, A. Nikroo, N. Rice, and S. M. Sepke, Phys. Plasmas **24**, 056302 (2017).

[65] R. Tommasini, J. E. Field, B. A. Hammel, O. L. Landen, S. W. Haan, C. Aracne-Ruddle, L. R. Benedetti, D. K. Bradley, D. A. Callahan, E. L. Dewald, T. Doeppner, M. J. Edwards, O. A. Hurricane, N. Izumi, O. A. Jones, T. Ma, N. B. Meezan, S. R. Nagel, J. R. Rygg, K. S. Segraves, M. Stadermann, R. J. Strauser, and R. P. J. Town, Phys. Plasmas **22**, 056315 (2015).

[66] R.H.H. Scott, D. S. Clark, D. K. Bradley, D. A. Callahan, M. J. Edwards, S.W. Haan, O. S. Jones, B. K. Spears, M. M. Marinak, R. P. J. Town, P. A. Norreys, and L. J. Suter, Phys. Rev. Lett. **110**, 075001 (2013).